

Figure 5 | Immunohistochemical study of F4/80, CD3, Ki-67, and type IV collagen (Col4). Mice were treated with chlorhexidine gluconate (CG) three times a week for 4 weeks. (a–d) F4/80, (e–h) CD3, (i–l) Ki67, and (m–p) Col4 staining in the peritoneum from (a, e, i, and m) phosphate-buffered saline (PBS)-injected wild-type (WT) mice, (b, f, j, and n) PBS-injected PTN knockout (KO) mice, (c, g, k, and o) CG-injected WT mice, (d, h, l, and p) CG-injected pleiotrophin (PTN)-KO mice. Arrows indicate positive cells. (q) The number of F4/80-positive cells per the number of total cells in the submesothelial area in mice. (r) The number of CD3-positive cells per the number of total cells in the submesothelial area in mice. (s) The number of Ki67-positive proliferated cells in the submesothelial area in mice. WT PBS: n = 5, KO PBS: n = 4, WT CG: n = 11, KO CG: n = 10. Mean ± s.e. **P < 0.01 vs. PBS-treated mice with the same genotype in Figure 5. #P < 0.05.

platelet-derived growth factor-AB.²⁶ A recent paper reveals that PTN expression is strongly associated with IFN- γ /JAK/STAT1 signaling.²⁷ Further investigations are necessary to elucidate the molecular mechanism of PTN induction. PTN is a ligand of the RPTP β / ζ ,^{12,28} ALK¹², and syndecan-3.¹² Our study showed that RPTP β / ζ was expressed in mesothelial cells, not in cultured fibroblasts, lymphocytes, or macrophages, and that syndecan-3 highly existed in mesothelial cells and was weakly expressed in fibroblasts and macrophages. ALK²⁹ was not detected in these cells. Taken together, PTN secreted by fibroblasts in submesothelial layer can have an effect on proliferation and migration mainly in mesothelial cells that express RPTP β / ζ and syndecan-3.³⁰ The role of PTN receptors in peritoneal fibrosis needs further clarification.

In this study, the role of PTN in peritoneal fibrosis was investigated by using PTN-deficient mice. Without PTN, inflammatory and profibrotic responses were significantly

reduced at 4 weeks after CG treatment, suggesting that PTN aggravates inflammation and fibrosis in the development of peritoneal fibrosis. Increased peritoneal permeability, examined by peritoneal equilibration tests, in CG-treated wild-type mice was almost completely ameliorated in CG-treated PTN knockout mice, suggesting that PTN can increase peritoneal permeability. Although CG-injected PTN knockout mice showed lower expression of COL1A1 and fibronectin than wild-type mice, the thickness of peritoneal membranes did not change between PTN-deficient mice and wild-type mice. The reason may come from similar expression levels of some other types of extracellular matrix such as collagen IV. Type IV collagen is abundantly deposited in peritoneal membrane.^{31,32} Although macrophage infiltration has been shown to be an important phenomenon in peritoneal fibrosis,³³ CG-treated PTN-deficient mice showed no apparent difference in macrophage infiltration compared with wild-type mice. T cells are also an important part of

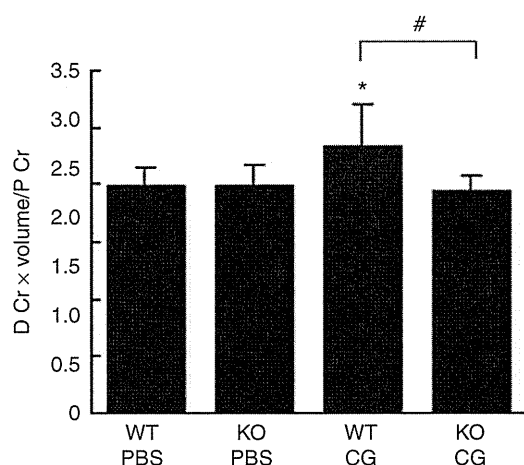


Figure 6 | Modified peritoneal equilibration test (PET). D Cr × volume/P Cr represents the creatinine (Cr) level of 7% glucose dialysate effluent (D) multiplied by volume divided by that of plasma (P) level in mice at 2 h retention. Chlorhexidine gluconate (CG)-injected wild-type (WT) mice showed increased D Cr × volume/P Cr compared with phosphate-buffered saline (PBS)-injected mice. Pleiotrophin (PTN)-knockout (KO) mice treated with CG showed reduced D Cr × volume/P Cr level compared with WT mice with CG. WT PBS: $n=3$, KO PBS: $n=6$, WT CG: $n=5$, KO CG: $n=7$. Mean ± s.e. * $P<0.05$ vs. PBS-treated mice with the same genotype in Figure 6. # $P<0.05$.

peritoneal membrane damage,^{34,35} and our results showed that T-cell infiltration was reduced in CG-treated PTN-deficient mice. PTN has been shown to induce expression of inflammatory cytokines in peripheral blood mononuclear cells.³⁶ The mechanism of T-cell infiltration by PTN is not clear, because RPTPβ/ζ mRNA nor syndecan-3 are not detected in cultured T-cell line. Downstream mediators of PTN need to be investigated in the future study. Cell proliferation was assessed by Ki-67 immunostaining.³⁷ PTN-deficient mice showed lower expression of Ki-67, indicating that cell proliferation in submesothelial layer was inhibited without PTN.

In conclusion, this study shows that PTN expression is upregulated in a mouse model of peritoneal fibrosis and is present in human peritoneal tissues and in peritoneal dialysate effluent, and that PTN secreted by fibroblasts or mesothelial cells can have a proliferative and chemotactic effect on mesothelial cells, and that PTN-deficient mice exhibit a weaker peritoneal membrane damage. These findings can be a help to elucidate a novel pathway in peritoneal fibrosis and suggest that PTN could be a promising biomarker against peritoneal damage.

MATERIALS AND METHODS

Patients

Patients who were admitted to Kyoto University Hospital for the diagnosis and treatment of renal disorders were enrolled under informed consent. This study was approved by the ethics committee on human research of Kyoto University Graduate School of Medicine. The parietal peritoneal samples were taken from the insertion site of a PD catheter located in the lumbar region as

biopsies at the beginning or ending of PD. Peritoneal dialysate effluents were obtained at the time of the exchange. Expression of PTN in peritoneal biopsy sample was assessed by the RT-PCR method. After RNA extraction by RNeasy mini kit (Qiagen, Valencia, CA), complementary DNA was generated using the SuperScript II Reverse Transcriptase (Invitrogen, Carlsbad, CA) according to the manufacturer's instruction. RT-PCR was performed using the following primers: forward, 5'-gggaagaagaccagt-gagt-3' and reverse, 5'-ctggttctcttctctccctgc-3'.

Induction of peritoneal fibrosis and phenotypic analysis

All animal experiments were approved by the animal experimentation committee of Kyoto University Graduate School of Medicine. Peritoneal fibrosis was induced in mice with the intraperitoneal injections of 0.3 ml of 0.1% CG in 15% ethanol and 85% PBS three times a week for 1, 2, 3, and 4 weeks as previously reported ($n=5$, each).³⁸ For evaluating dose-response, mice were administered 0.3 ml of 0.01% and 0.03% CG in 15% ethanol and 85% PBS three times a week for 4 weeks. Control mice received intraperitoneal injection of PBS. Mice were killed under pentobarbital anesthesia, and peritoneal tissues were obtained from the upper portion of the parietal peritoneum to avoid injured peritoneum by repeated injections.

For dialysis fluid infusion, silicone port catheters with two cuffs were used (PennyPort MMP-4S; Access Technologies, Skokie, IL). After mice were anesthetized under pentobarbital, an incision was made in the skin of the back and left lumbar portion. Peritoneal membrane was pricked with a 20-Gy needle to make a small hole. The catheter port was implanted under the skin of the back and the catheters were inserted along the needle hole. A catheter port was placed subcutaneously on the back. One milliliter of PDFs (Perisate; JMS, Hiroshima, Japan) containing 7% PD solution or PBS were administered intraperitoneally via a catheter port using a 26-Gy needle every day for 4 weeks ($n=5$, each). PTN-deficient mice (C57BL/6J background) were generated as described previously.¹³

Modified peritoneal equilibration test

Modified peritoneal equilibration test was conducted to determine the peritoneal permeability. Wild-type or PTN knockout mice were injected with PBS or CG ($n=5$, each) three times for 2 weeks, and were then administered intraperitoneal injection of 3 ml of 7% glucose dialysis solution (Perisate; JMS). After 2 h of retention, dialysis fluids were collected and blood samples were withdrawn. Serum and dialysate creatinine levels were measured by using the enzymatic method (SRL, Tokyo, Japan).

Affymetrix gene chip array

Wild-type mice were subjected to peritoneal fibrosis with the intraperitoneal injections of 0.3 ml of 0.1% CG in 15% ethanol and 85% PBS three times a week for 3 weeks ($n=3$). As control, PBS-treated wild-type mice were used ($n=3$). Total RNA from the parietal peritoneum at day 21 was extracted by RNeasy Mini Kit (Qiagen) in these mice.³⁹ Complementary RNA probes were generated using the GeneChip Expression 3'-Amplification Reagents for IVT Labeling Kit (Applied Biosystems, Foster city, CA) and each sample was hybridized to an Affymetrix mouse genome 430 2.0 array at TAKARA Bio (Shiga, Japan). After washing, the genechips were scanned by a GeneChip Scanner 3000. Data normalization, log transformation, statistical analysis, and pattern study were performed with the GeneChip Operating Software.

Histology and immunohistochemistry

Peritoneal membrane sections were fixed with 4% buffered paraformaldehyde and embedded in paraffin. Sections (1 μm thick) were stained with Masson's trichrome.⁴⁰ We measured the thickness of the fibrotic submesothelial zone above the abdominal muscle layer in cross-sections as described previously,⁴¹ by using MetaMorph software (Molecular Devices, Downingtown, PA). Ten different points were examined by two investigators without knowledge of the origin of the slides. The results were expressed as the average peritoneal membrane thickness. For immunohistochemical analyses of PTN, collagen type IV, F4/80, CD3, and Ki-67 in mice, the sections were processed as described.⁴⁰ After antigen retrieval, the samples were incubated with rabbit polyclonal anti-PTN antibody (ProteinTech Group, Chicago, IL), rabbit polyclonal anti-mouse collagen type IV antibody (Millipore, Billerica, MA), rat monoclonal anti-F4/80 antibody (Serotec, Oxford, UK), rabbit polyclonal anti-CD3 antibody (DAKO, Glostrup, Denmark), and rat monoclonal anti-Ki-67 antibody (DAKO). After incubation with horseradish peroxidase-conjugated secondary antibodies, the specimens were developed using 3,3'-diaminobenzidine tetrahydrochloride. For immunohistochemical study of human PTN, we used a rabbit polyclonal anti-PTN antibody (Abcam, Cambridge, UK) as a primary antibody.

Real-time PCR analysis

Quantitative real-time PCR was performed using Premix Ex Taq (TAKARA Bio) on an Applied Biosystems 7300 real-time PCR system (Applied Biosystems) or a StepOnePlus system (Applied Biosystems), as described previously with some modification.³⁹ To determine mouse PTN, Ptpz1, TGF- β 1, connective tissue growth factor, COL1A1, COL4A1, fibronectin, and IL-1 β and tumor necrosis factor- α expression levels, gene-specific primers and probes were used. Primers and probe sequences are listed in Supplementary Table S1 online. Expression of each mRNA was normalized for glyceraldehyde-3-phosphate dehydrogenase using TaqMan Rodent glyceraldehyde-3-phosphate dehydrogenase control reagents (Applied Biosystems).

Western blot analysis

Western blot analysis was performed as described.³⁹ Filters transferred onto protein extracts or peritoneal dialysate effluents were incubated with rabbit polyclonal anti-PTN antibody (ProteinTech Group) and mouse monoclonal anti-glyceraldehyde-3-phosphate dehydrogenase antibody (Santa Cruz Biotechnology, Santa Cruz, CA). Immunoblots were then developed using a chemiluminescence kit (GE healthcare, Piscataway, NJ).

Cell culture

Mouse peritoneal mesothelial cells were obtained using a standard trypsin/ethylenediaminetetraacetic acid digestion method from the peritoneal wall of adult male C57BL/6J mice.^{42,43} The excised peritoneal flap was cut into small pieces and then incubated, with constant agitation, with 0.25% trypsin and 1 mmol/l ethylenediaminetetraacetic acid (Invitrogen) for 15 min at 37 °C. The released cells were centrifuged at 1200 r.p.m. for 5 min and cultured with Dulbecco's Modified Eagle Medium (DMEM D6046; Sigma-Aldrich, St Louis, MI) supplemented with 10% fetal bovine serum (FBS), penicillin (100 U/ml), streptomycin (100 $\mu\text{g}/\text{ml}$), and amphotericin B (25 ng/ml). NIH3T3 fibroblasts, RAW264.7 cells, and bEnd.3 cells were obtained from American Type Culture Collection (Manassas,

VA). BW5147 cells were provided by Health Science Research Bank (Sennan, Osaka, Japan) and BCL1-B20 cells were provided by the RIKEN BRC through the National Bio-Resource Project of the Ministry of Education, Culture, Sports, Science and Technology, Japan. BCL1-B20 cells were cultured with RPMI1640 (Sigma) with 10% FBS. Other cells were cultured with DMEM with 10% FBS.

Proliferation assay in cultured mesothelial cells was performed with ³H-thymidine as described previously.⁴⁴ Briefly, mesothelial cells were plated on 24-well plates ($n=6$, each group) and incubated with DMEM containing 0.3% FBS for the 24 h. Cell proliferation was studied in the presence of 1 ng/ml of recombinant human PTN (R&D Systems, Minneapolis, MN), 10 ng/ml of recombinant human platelet-derived growth factor-BB (BD Biosciences, San Jose, CA), 10^{-6} mol/l of angiotensin II (Peptide Institute, Osaka, Japan), 100 ng/ml of recombinant human endothelial growth factor (PeproTech EC, London, UK), or vehicle (PBS) for 24 h with DMEM containing 0.3% FBS. ³H-thymidine was added simultaneously with the above-described agents. Migration assay was performed as described previously.⁴⁵ In brief, migration of mesothelial cells was analyzed by modified Boyden chamber method using 96-well chemotaxis chambers. In the upper chambers, mesothelial cells were placed with DMEM containing 0.02% bovine serum albumin. In the lower chambers, there were serum-free DMEM containing PTN (1 ng/ml), platelet-derived growth factor-BB (50 ng/ml), angiotensin II (10^{-6} mol/l), or endothelial growth factor (100 ng/ml). The cells were incubated for 4 h and the filters were stained with 0.5% Coomassie Brilliant Blue R250 (Nacalai Tesque, Kyoto, Japan) in 50% methanol, 40% water, and 10% acetic acid ($n=6$, each).

Statistical analysis

Data are expressed as the mean \pm s.e. Statistical analysis was performed using one-way analysis of variance as appropriate. A P -value <0.05 was considered statistically significant.

DISCLOSURE

All the authors declared no competing interests.

ACKNOWLEDGMENTS

We gratefully acknowledge M Fujimoto and Y Sakashita and other lab members for technical assistance, and A Yamamoto for secretarial assistance. This work was supported in part by research grants from the Japanese Ministry of Education, Culture, Sports, Science and Technology, the Japanese Ministry of Health, Labour and Welfare, and Japan Baxter PD Fund.

SUPPLEMENTARY MATERIAL

Table S1. TaqMan primers and probe sequences.

Supplementary material is linked to the online version of the paper at <http://www.nature.com/ki>

REFERENCES

1. Ledebro I, Ronco C. The best dialysis therapy? Results from an international survey among nephrology professionals. *NDT Plus* 2008; **1**: 403–408.
2. Saxena R. Pathogenesis and treatment of peritoneal membrane failure. *Pediatr Nephrol* 2008; **23**: 695–703.
3. Yung S, Chan TM. Preventing peritoneal fibrosis—insights from the laboratory. *Perit Dial Int* 2003; **23**(S2): S37–S41.
4. Pecoits-Filho R, Araujo MR, Lindholm B *et al.* Plasma and dialysate IL-6 and VEGF concentrations are associated with high peritoneal solute transport rate. *Nephrol Dial Transplant* 2002; **17**: 1480–1486.
5. Lai KN, Lai KB, Szeto CC *et al.* Growth factors in continuous ambulatory peritoneal dialysis effluent. Their relation with peritoneal transport of small solutes. *Am J Nephrol* 1999; **19**: 416–422.

6. Oh KH, Jung JY, Yoon MO *et al.* Intra-peritoneal interleukin-6 system is a potent determinant of the baseline peritoneal solute transport in incident peritoneal dialysis patients. *Nephrol Dial Transplant* 2010; **25**: 1639–1646.
7. Margetts PJ, Kolb M, Galt T *et al.* Gene transfer of transforming growth factor- β 1 to the rat peritoneum: effects on membrane function. *J Am Soc Nephrol* 2001; **12**: 2029–2039.
8. Margetts PJ, Kolb M, Yu L *et al.* Inflammatory cytokines, angiogenesis, and fibrosis in the rat peritoneum. *Am J Pathol* 2002; **160**: 2285–2294.
9. Aroeira LS, Aguilera A, Selgas R *et al.* Mesenchymal conversion of mesothelial cells as a mechanism responsible for high solute transport rate in peritoneal dialysis: role of vascular endothelial growth factor. *Am J Kidney Dis* 2005; **46**: 938–948.
10. Zakaria el R, Matheson PJ, Hurt RT *et al.* Chronic infusion of sterile peritoneal dialysis solution abrogates enhanced peritoneal gene expression responses to chronic peritoneal catheter presence. *Adv Perit Dial* 2008; **24**: 7–15.
11. Deuel TF, Zhang N, Yeh HJ *et al.* Pleiotrophin: a cytokine with diverse functions and a novel signaling pathway. *Arch Biochem Biophys* 2002; **397**: 162–171.
12. Jin L, Jianghai C, Juan L *et al.* Pleiotrophin and peripheral nerve injury. *Neurosurg Rev* 2009; **32**: 387–393.
13. Muramatsu H, Zou P, Kurosawa N *et al.* Female infertility in mice deficient in midkine and pleiotrophin, which form a distinct family of growth factors. *Genes Cells* 2006; **11**: 1405–1417.
14. Lu KV, Jong KA, Kim GY *et al.* Differential induction of glioblastoma migration and growth by two forms of pleiotrophin. *J Biol Chem* 2005; **280**: 26953–26964.
15. Milner PG, Li YS, Hoffman RM *et al.* A novel 17 kD heparin-binding growth factor (HBGF-8) in bovine uterus: purification and N-terminal amino acid sequence. *Biochem Biophys Res Commun* 1989; **165**: 1096–1103.
16. Rauvala H. An 18-kd heparin-binding protein of developing brain that is distinct from fibroblast growth factors. *EMBO J* 1989; **8**: 2933–2941.
17. Sakurai H, Bush KT, Nigam SK. Identification of pleiotrophin as a mesenchymal factor involved in ureteric bud branching morphogenesis. *Development* 2001; **128**: 3283–3293.
18. Amet LE, Lauri SE, Hienola A *et al.* Enhanced hippocampal long-term potentiation in mice lacking heparin-binding growth-associated molecule. *Mol Cell Neurosci* 2001; **17**: 1014–1024.
19. Ochiai K, Muramatsu H, Yamamoto S *et al.* The role of midkine and pleiotrophin in liver regeneration. *Liver Int* 2004; **24**: 484–491.
20. Yamamoto R, Nakayama M, Hasegawa T *et al.* High-transport membrane is a risk factor for encapsulating peritoneal sclerosis developing after long-term continuous ambulatory peritoneal dialysis treatment. *Adv Perit Dial* 2002; **18**: 131–134.
21. Kawanishi H, Moriishi M. Encapsulating peritoneal sclerosis: prevention and treatment. *Perit Dial Int* 2007; **27**(S2): S289–S292.
22. Kawanishi H, Fujimori A, Tsuchida K *et al.* Markers in peritoneal effluent for withdrawal from peritoneal dialysis: multicenter prospective study in Japan. *Adv Perit Dial* 2005; **21**: 134–138.
23. Kawanishi H, Harada Y, Noriyuki T *et al.* Treatment options for encapsulating peritoneal sclerosis based on progressive stage. *Adv Perit Dial* 2001; **17**: 200–204.
24. Xu X, Rivkind A, Pappo O *et al.* Role of mast cells and myofibroblasts in human peritoneal adhesion formation. *Ann Surg* 2002; **236**: 593–601.
25. Dreyfus J, Brunet-de Carvalho N, Duprez D *et al.* HB-GAM/pleiotrophin: localization of mRNA and protein in the chicken developing leg. *Int J Dev Biol* 1998; **42**: 189–198.
26. Li YS, Gurrieri M, Deuel TF. Pleiotrophin gene expression is highly restricted and is regulated by platelet-derived growth factor. *Biochem Biophys Res Commun* 1992; **184**: 427–432.
27. Li F, Tian F, Wang L *et al.* Pleiotrophin (PTN) is expressed in vascularized human atherosclerotic plaques: IFN- γ /JAK/STAT1 signaling is critical for the expression of PTN in macrophages. *FASEB J* 2010; **24**: 810–822.
28. Meng K, Rodriguez-Pena A, Dimitrov T *et al.* Pleiotrophin signals increased tyrosine phosphorylation of β -catenin through inactivation of the intrinsic catalytic activity of the receptor-type protein tyrosine phosphatase β / ζ . *Proc Natl Acad Sci U S A* 2000; **97**: 2603–2608.
29. Stoica GE, Kuo A, Aigner A *et al.* Identification of anaplastic lymphoma kinase as a receptor for the growth factor pleiotrophin. *J Biol Chem* 2001; **276**: 16772–16779.
30. Raulo E, Chernousov MA, Carey DJ *et al.* Isolation of a neuronal cell surface receptor of heparin binding growth-associated molecule (HB-GAM). Identification as N-syndecan (syndecan-3). *J Biol Chem* 1994; **269**: 12999–13004.
31. Mateijsen MA, van der Wal AC, Hendriks PM *et al.* Vascular and interstitial changes in the peritoneum of CAPD patients with peritoneal sclerosis. *Perit Dial Int* 1999; **19**: 517–525.
32. Saito H, Kitamoto M, Kato K *et al.* Tissue factor and factor V involvement in rat peritoneal fibrosis. *Perit Dial Int* 2009; **29**: 340–351.
33. Schilte MN, Celie JW, Wee PM *et al.* Factors contributing to peritoneal tissue remodeling in peritoneal dialysis. *Perit Dial Int* 2009; **29**: 605–617.
34. Glik A, Douvdevani A. T lymphocytes: the 'cellular' arm of acquired immunity in the peritoneum. *Perit Dial Int* 2006; **26**: 438–448.
35. Devuyt O, Margetts PJ, Topley N. The pathophysiology of the peritoneal membrane. *J Am Soc Nephrol* 2010; **21**: 1077–1085.
36. Achour A, M'Bika JB, Baudouin F *et al.* Pleiotrophin induces expression of inflammatory cytokines in peripheral blood mononuclear cells. *Biochimie* 2008; **90**: 1791–1795.
37. Endl E, Gerdes J. The Ki-67 Protein: Fascinating forms and an unknown function. *Exp Cell Res* 2000; **257**: 231–237.
38. Ishii Y, Sawada T, Shimizu A *et al.* An experimental sclerosing encapsulating peritonitis model in mice. *Nephrol Dial Transplant* 2001; **16**: 1262–1266.
39. Yokoi H, Mukoyama M, Mori K *et al.* Overexpression of connective tissue growth factor in podocytes worsens diabetic nephropathy in mice. *Kidney Int* 2008; **73**: 446–455.
40. Yokoi H, Mukoyama M, Nagae T *et al.* Reduction in connective tissue growth factor by antisense treatment ameliorates renal tubulointerstitial fibrosis. *J Am Soc Nephrol* 2004; **15**: 1430–1440.
41. Yoshio Y, Miyazaki M, Abe K *et al.* TNP-470, an angiogenesis inhibitor, suppresses the progression of peritoneal fibrosis in mouse experimental model. *Kidney Int* 2004; **66**: 1677–1685.
42. Tamura M, Osajima A, Nakayama S *et al.* High glucose levels inhibit focal adhesion kinase-mediated wound healing of rat peritoneal mesothelial cells. *Kidney Int* 2003; **63**: 722–731.
43. Yung S, Li FK, Chan TM. Peritoneal mesothelial cell culture and biology. *Perit Dial Int* 2006; **26**: 162–173.
44. Suganami T, Mukoyama M, Sugawara A *et al.* Overexpression of brain natriuretic peptide in mice ameliorates immune-mediated renal injury. *J Am Soc Nephrol* 2001; **12**: 2652–2663.
45. Sawai K, Mori K, Mukoyama M *et al.* Angiogenic protein Cyr61 is expressed by podocytes in anti-Thy-1 glomerulonephritis. *J Am Soc Nephrol* 2003; **14**: 1154–1163.

Exacerbation of diabetic nephropathy by hyperlipidaemia is mediated by Toll-like receptor 4 in mice

T. Kuwabara · K. Mori · M. Mukoyama ·
M. Kasahara · H. Yokoi · Y. Saito · Y. Ogawa ·
H. Imamaki · T. Kawanishi · A. Ishii · K. Koga ·
K. P. Mori · Y. Kato · A. Sugawara · K. Nakao

Received: 3 February 2012 / Accepted: 4 April 2012 / Published online: 19 May 2012
© Springer-Verlag 2012

Abstract

Aims/hypothesis Hyperlipidaemia is an independent risk factor for the progression of diabetic nephropathy, but its molecular mechanism remains elusive. We investigated in mice how diabetes and hyperlipidaemia cause renal lesions separately and in combination, and the involvement of Toll-like receptor 4 (TLR4) in the process.

Methods Diabetes was induced in wild-type (WT) and *Tlr4* knockout (KO) mice by intraperitoneal injection of streptozotocin (STZ). At 2 weeks after STZ injection, normal diet was substituted with a high-fat diet (HFD). Functional and histological analyses were carried out 6 weeks later.

Results Compared with treatment with STZ or HFD alone, treatment of WT mice with both STZ and HFD markedly aggravated nephropathy, as indicated by an increase in albuminuria, mesangial expansion, infiltration of macrophages and upregulation of pro-inflammatory and extracellular-matrix-associated gene expression in glomeruli. In *Tlr4* KO mice, the addition of an HFD to STZ had almost no effects on the variables measured. Production of protein S100 calcium binding protein A8 (calgranulin A; S100A8), a potent ligand

for TLR4, was observed in abundance in macrophages infiltrating STZ-HFD WT glomeruli and in glomeruli of diabetic nephropathy patients. High-glucose and fatty acid treatment synergistically upregulated *S100a8* gene expression in macrophages from WT mice, but not from KO mice. As putative downstream targets of TLR4, phosphorylation of interferon regulatory factor 3 (IRF3) was enhanced in kidneys of WT mice co-treated with STZ and HFD.

Conclusions/interpretation Activation of S100A8/TLR4 signalling was elucidated in an animal model of diabetic glomerular injury accompanied with hyperlipidaemia, which may provide novel therapeutic targets in progressive diabetic nephropathy.

Keywords Diabetic nephropathy · Glomerulus · High-fat diet · Hyperlipidaemia · Macrophages · S100A8 · TLR4

Abbreviations

BMDMs	Bone marrow-derived macrophages
C _t	Cycle threshold
CTGF	Connective tissue growth factor
ECM	Extracellular matrix
ESRD	End-stage renal disease
GAPDH	Glyceraldehyde-3-phosphate dehydrogenase
HFD	High-fat diet
IKB	Inhibitor κ B
IRF3	Interferon regulatory factor 3
JNK	c-Jun N-terminal kinase
KO	Knockout
MAC-2	Lectin galactoside-binding, soluble, 3
MYD88	Myeloid differentiation primary response gene (88)
ND	Normal diet
nSTZ	non-STZ
PAS	periodic acid–Schiff

Electronic supplementary material The online version of this article (doi:10.1007/s00125-012-2578-1) contains peer-reviewed but unedited supplementary material, which is available to authorised users.

T. Kuwabara · K. Mori (✉) · M. Mukoyama · M. Kasahara ·
H. Yokoi · Y. Saito · H. Imamaki · T. Kawanishi · A. Ishii ·
K. Koga · K. P. Mori · Y. Kato · K. Nakao
Department of Medicine and Clinical Science,
Kyoto University Graduate School of Medicine,
54 Shogoin Kawaharacho, Sakyo-ku,
Kyoto 606-8507, Japan
e-mail: keyem@kuhp.kyoto-u.ac.jp

Y. Ogawa · A. Sugawara
Department of Nephrology, Osaka Redcross Hospital,
Osaka, Japan

S100A8	S100 calcium binding protein A8
S100A9	S100 calcium binding protein A9
STZ	Streptozotocin
TLR	Toll-like receptor
TRIF	TIR-domain-containing adapter-inducing interferon- β
WT	Wild-type

Introduction

Diabetic nephropathy is one of the most prevalent causes of end-stage renal disease (ESRD) [1]. Despite progress in pharmacological strategies to control diabetes, hypertension and other metabolic abnormalities, the number of patients entering ESRD because of diabetic nephropathy remains extremely high, and the development of new classes of therapeutic reagents is eagerly anticipated [2]. During recent decades, the pathophysiology of diabetic nephropathy has become complex and serious because of coexisting lifestyle-related disorders, such as hyperlipidaemia, hypertension and obesity [3]. In fact, hyperlipidaemia is an independent risk factor for the progression of diabetic nephropathy in both type 1 and type 2 diabetes [4, 5], but the underlying molecular mechanism remains elusive [6].

Toll-like receptors (TLRs) are a family of receptors that play a critical role in the innate immune system by activating pro-inflammatory signalling pathways in response to molecular patterns synthesised by microorganisms [7]. TLR4, one of the best-characterised TLRs, binds with lipopolysaccharide from Gram-negative bacterial cell walls and with several endogenous ligands [7]. TLR4 also plays an important role in various kidney disorders, such as glomerulonephritis, renal ischaemia and diabetic tubular inflammation [8–13], but the role of TLR4 in diabetic glomerular injury and hyperlipidaemia-induced kidney damage remains largely unknown.

In the current study, TLR4 and its novel endogenous ligand S100 calcium binding protein A8 (S100A8) emerged as candidate molecules involved in the progression of diabetic nephropathy by our microarray analysis performed in two different types of diabetic mouse models. Furthermore, we examined the effects of high-fat diet (HFD) feeding on streptozotocin (STZ)-induced diabetes in *Tlr4* knockout (KO) and wild-type (WT) mice in order to elucidate the mechanism for the progression of diabetic nephropathy caused by hyperlipidaemia.

Methods

Experimental animals Male *Tlr4* KO [14] and WT mice with a C57BL/6 J genetic background were studied. To generate a mouse model of diabetes complicated by hyperlipidaemia, 8-week-old mice were intraperitoneally injected

with STZ (100 mg/kg body weight in citrate buffer, pH 4.0; Sigma-Aldrich, St Louis, MO, USA) or vehicle for 3 consecutive days. After 2 weeks, normal diet (ND; NMF, 14.7 kJ/g [3.5 kcal/g], 13% of energy as fat; Oriental Yeast, Tokyo, Japan) was substituted with an HFD (D12451, 19.7 kJ/g [4.7 kcal/g], 45% of energy as fat; Research Diets, New Brunswick, NJ, USA) in subgroups of animals, and all were killed for analysis at 8 weeks after STZ treatment. In another set of experiments, 8-week-old male *db/db* mice (on a BKS genetic background; Japan Clea, Tokyo, Japan) were randomly assigned to ND or HFD (D12492, 21.8 kJ/g [5.2 kcal/g], 60% of energy as fat; Research Diets) groups and followed for 4 weeks. All animal experiments were conducted in accordance with the Guidelines for Animal Research Committee of Kyoto University Graduate School of Medicine.

Human biopsy samples Human kidney samples obtained at renal biopsy carried out in our department were used for immunohistochemistry. The human study protocol was approved by the Ethical Committee on Human Research of Kyoto University Graduate School of Medicine. All participants gave written informed consent.

Measurement of metabolic variables Metabolic variables were measured as described previously [15, 16]. Briefly, blood pressure was measured by indirect tail-cuff method (Muromachi Kikai, Tokyo, Japan). Urine samples were collected with metabolism cages, and urinary albumin was measured with competitive ELISA (Exocell, Philadelphia, PA, USA). Serum and urinary creatinine levels were assayed by enzymatic method (SRL, Tokyo, Japan) [17]. Plasma glucose, triacylglycerol and total cholesterol levels were measured, under conditions of ad libitum feeding, using an enzymatic method (Wako Pure Chemicals, Osaka, Japan). Plasma insulin levels were measured by enzyme immunoassay (Morinaga, Tokyo, Japan). For measurement of tissue triacylglycerol content, lipids were extracted with isopropyl alcohol/heptane (1:1 [vol./vol.]) from frozen kidney samples. After evaporating the solvent, lipids were resuspended in 99.5% ethanol and triacylglycerol contents were measured as described above.

Real-time quantitative RT-PCR Total RNA was extracted with TRIzol reagent (Invitrogen, Carlsbad, CA, USA) and cDNA in each sample was synthesised using the High Capacity cDNA Reverse Transcription Kit (Applied Biosystems, Foster City, CA, USA) from mouse kidneys and glomeruli isolated by graded sieving method [18, 19]. TaqMan real-time PCR was performed using Premix Ex Taq (Takara Bio, Otsu, Japan) and StepOnePlus Real Time PCR System (Applied Biosystems, Foster City, CA, USA). See Electronic supplementary material (ESM) Table 1 for primer

and probe sequences. Expression levels of all genes were normalised by *Gapdh* (internal control) levels. The mean expression level in whole kidney of WT non-treated control mice was arbitrarily defined as 1.0.

Histological analysis Periodic acid–Schiff (PAS) staining of the mesangial area and immunohistochemistry of S100A8 (requiring antigen retrieval by citrate buffer) and lectin, galactoside-binding, soluble, 3 (MAC-2 or LGALS3) [18] were carried out using kidney sections (thickness 4 μ m) fixed with 4% buffered paraformaldehyde. Nuclei were counterstained with haematoxylin. All the primary antibodies used in this study are shown in ESM Table 2. For double staining, primary antibody for S100A8 was visualised with DyLight-conjugated secondary antibody (Takara Bio, Otsu, Japan). Immunofluorescence of podocin (or NPHS2) was performed with snap-frozen cryostat sections (4 μ m), pre-treated with cold acetone and 0.1% Triton-X100, and with primary and FITC-labelled secondary antibodies. Photographs were taken by a fluorescence microscope (IX81-PAFM; Olympus, Tokyo, Japan). Mesangial and podocin-positive areas of more than ten glomeruli from the outer cortex were measured quantitatively to obtain an average for each mouse using MetaMorph 7.5 software (Molecular Devices, Downingtown, PA, USA). Formalin-fixed, snap-frozen sections (10 μ m) were stained with Oil Red O to evaluate lipid-droplet-positive areas.

Microarray analysis Two different types of diabetic mouse model were employed for microarray analysis. Male A-ZIP/F-1 heterozygous transgenic mice and control male FVB/N littermates were used at 10 months of age, when A-ZIP/F-1 mice exhibited diabetic nephropathy with massive proteinuria [20]. The other model was STZ-induced, insulin-dependent, diabetic C57BL/6 J male mice (Japan Clea) in which diabetes was induced at 9 weeks of age by single intraperitoneal injection of STZ (180 mg/kg); mice were analysed 8 weeks later. We essentially followed the procedures described in detail in the GeneChip Eukaryotic Target Preparation & Hybridization Manual (Affymetrix, Santa Clara, CA, USA). In brief, cDNA was synthesised and biotin-labelled cRNA was produced through in vitro transcription labelling Kit (Affymetrix). Fragmented cRNA was hybridised to GeneChip Mouse Genome 430 2.0 Array (Affymetrix) at 45°C for 16 h. The samples were washed and stained according to the manufacturer's protocol on GeneChip Fluidic Station 450 (Affymetrix) and scanned on GeneChip Scanner 3000 (Affymetrix).

PCR array analysis To eliminate contaminating genomic DNA, total RNA extracted from kidney samples was purified using RNeasy Mini Kit (QIAGEN Sciences, Maryland, MD, USA). First-strand cDNA was synthesised from total RNA using the RT2 first-strand kit (SABiosciences, Frederick, MD,

USA). The mouse TLR-signalling pathway RT2 Profiler PCR plate (PAMM-018, SABiosciences) and StepOnePlus were used for amplification of cDNA. The analysis used 96 well plates containing gene-specific primer sets for 84 relevant TLR pathway genes, five housekeeping genes and two negative controls. The cycle threshold (C_t) was determined for each sample and normalised to the average C_t of the five housekeeping genes. The comparative ΔC_t method (SABiosciences) was used to calculate relative gene expression.

Western blot analysis Proteins extracted from kidney samples were separated by SDS-PAGE, transferred onto PVDF membranes, incubated with primary antibodies and detected with peroxidase-conjugated secondary antibodies and chemiluminescence [19]. Glyceraldehyde-3-phosphate dehydrogenase (GAPDH) was used as an internal control.

Cultured macrophages Palmitate (Sigma-Aldrich) was solubilised in ethanol, and combined with fatty-acid-free, low endotoxin, bovine serum albumin (Sigma-Aldrich) at a molar ratio of 10:1 in serum-free medium. Polymyxin B (10 μ g/ml, Nacalai Tesque, Kyoto, Japan) was added to each well to minimise contamination of endotoxin. Bone marrow-derived macrophages (BMDMs) were generated from mice as described previously [21]. Briefly, following lysis of erythrocytes, bone marrow cells were resuspended in medium containing 20% fetal calf serum and 50 ng/ml recombinant human macrophage colony-stimulating factor, and cultured at 37°C in 5% CO₂ atmosphere. On day 6, the medium was replaced with fresh medium containing 5.6 mmol/l or 25 mmol/l glucose. On day 7, macrophages were incubated with palmitate or vehicle for 24 h. Total RNA from cells was extracted with RNeasy Mini Kit, and mRNA expression levels of *S100a8* and *Tlr4* were determined by TaqMan real-time RT-PCR.

Statistical analysis Data are expressed as means \pm SEM. Differences between multiple groups were assessed by two-way factorial ANOVA with Bonferroni's post test. Comparisons between two groups were carried out by unpaired Student's *t* test. Statistical significance was defined as $p < 0.05$.

Results

Changes of metabolic variables and albuminuria in WT diabetic mice given a fat-rich diet Metabolic variables of non-STZ (nSTZ)-HFD, STZ-ND, STZ-HFD and control nSTZ-ND groups of WT mice are shown in Table 1. HFD treatment (compared with ND) in nSTZ mice caused significant elevation of body weight, plasma glucose, insulin,

Table 1 Metabolic data of WT and *Tlr4* KO mice at 8 weeks after STZ injection

Variable	WT				KO			
	nSTZ-ND	nSTZ-HFD	STZ-ND	STZ-HFD	nSTZ-ND	nSTZ-HFD	STZ-ND	STZ-HFD
Number of animals	6	4	8	11	4	4	5	8
Body weight (g)	27.7±1.0	33.7±0.5**	20.0±0.9**	22.1±0.5**.§§§	34.9±2.4†	39.6±1.4†	22.0±1.3**	23.3±0.6***.§§§
Blood pressure (mmHg)								
Systolic	101±2	104±2	98±1	100±1	103±2	103±2	96±1*	101±2
Diastolic	56±2	57±3	52±2	56±2	55±1	57±2	50±1*	53±1
Kidney weight (% body weight)	0.5±0.0	1.0±0.0**	1.7±0.1**	1.8±0.1**.§§§	1.0±0.1†††	2.2±0.2***.††	1.9±0.2***	1.9±0.1***
Plasma glucose (mmol/l)	9.5±1.6	14.0±0.4*	40.0±3.9**	32.9±1.8**.§	10.4±1.1	12.7±2.3	36.0±7.7*	31.8±2.3***.§§
HbA _{1c} (%)	3.4±0.1	5.3±0.1**	9.6±0.6**	9.9±0.5**.§	3.0±0.3	4.9±0.2**	9.4±1.1**	10.3±0.3***.§§§
HbA _{1c} (mmol/mol)	13.3±1.4	34.1±0.7**	81.8±6.5**	84.6±5.1**.§	9.0±2.8	29.5±2.5**	78.9±12.5**	89.4±3.2***.§§§
Plasma insulin (pmol/l)	133±16	256±21**	10±2**	12±2**.§§§	238±43	336±33	12±5**	12±5**.§§§
Plasma triacylglycerol (mmol/l)	0.99±0.02	1.20±0.03**	2.36±1.01*	5.48±1.56*.§	1.74±0.32	1.42±0.11	3.12±1.56	7.64±1.58**.§§
Plasma total cholesterol (mmol/l)	1.5±0.4	3.4±0.3*	5.1±0.8*	5.2±0.5**	1.9±0.4	3.4±0.2*	3.8±0.6*	5.9±0.4**.§§.‡
Serum creatinine (μmol/l)	8.0±1.8	8.8±0.1	10.6±0.9	15.9±5.3	8.8±0.1	8.0±0.1††	10.6±1.8	8.0±0.1

Data are means±SEM

Blood was collected with mice fed ad libitum

* $p < 0.05$, ** $p < 0.01$, *** $p < 0.001$ vs nSTZ-ND; † $p < 0.05$, †† $p < 0.01$, ††† $p < 0.001$ vs similarly treated group of WT; ‡ $p < 0.05$ vs STZ-ND; § $p < 0.05$, §§ $p < 0.01$, §§§ $p < 0.001$ vs nSTZ-HFD

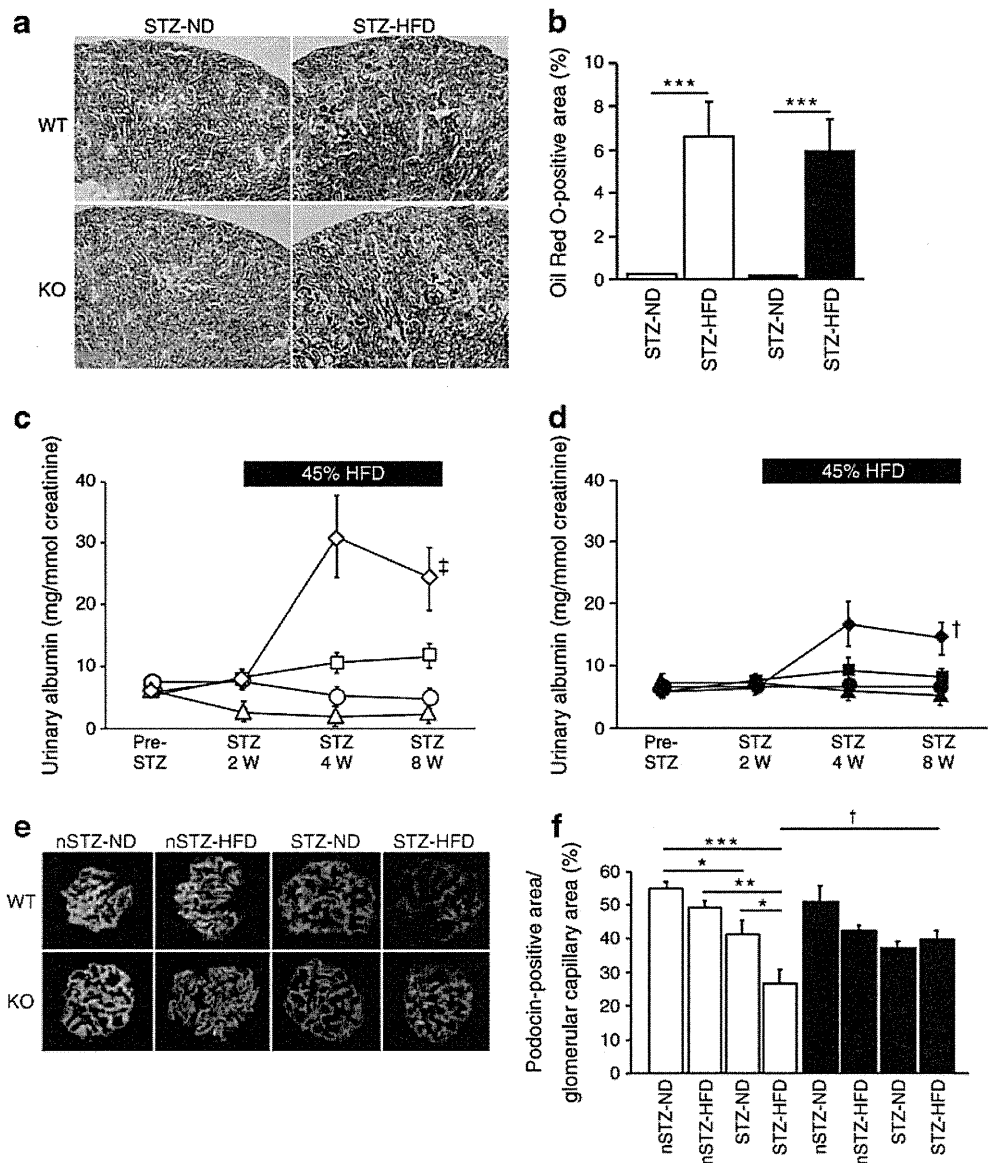
triacylglycerol and total cholesterol levels. STZ treatment (compared with nSTZ) in ND mice caused significant body weight loss and significant elevation of plasma glucose, triacylglycerol and total cholesterol levels. Treatment of STZ mice with HFD resulted in large exacerbation of hypertriacylglycerolaemia (by 2.3-fold) without significant changes in other above-mentioned variables (Table 1). Consistently, renal lipid deposition in STZ-HFD mice was markedly increased compared with STZ-ND mice (Fig. 1a, b). Blood pressures were not significantly different among the four treatment groups (Table 1).

Concerning albuminuria, one of the representative abnormalities that characterise diabetic nephropathy [2], albumin excretion in STZ-ND was elevated by 2.3-fold at 8 weeks compared with nSTZ-ND mice (Fig. 1c). The addition of HFD to STZ mice further enhanced albuminuria approximately twofold. To investigate podocyte injury, we investigated whether podocin protein production is decreased in the glomeruli of STZ-HFD mice [19]. Glomerular podocin level was significantly reduced in STZ-ND compared with nSTZ-ND and was lowest in STZ-HFD (Fig. 1e, f). Also, in obese, type 2 diabetic *db/db* mice, albuminuria was exaggerated by HFD (ESM Fig. 1). To summarise, treatment of WT mice with a combination of HFD and STZ resulted in

marked enhancement of hypertriglycerolaemia, renal lipid deposition, podocyte damage and albumin excretion.

Gene expression analysis of pro-inflammatory and extracellular-matrix-associated genes in whole kidney and glomeruli and histological examination We measured mRNA levels of pro-inflammatory and extracellular matrix (ECM)-associated genes both in whole kidney and isolated glomeruli (Fig. 2, ESM Table 3). The former set of genes included *Mcp1* (also known as *Ccl2*, encoding monocyte chemoattractant protein-1 [MCP1]), *F4/80* (also known as *Emr1*), *Cd68*, *Tnfa* (also known as *Tnf* [encoding TNF]), *Pail* (also known as *Serpine1* [encoding plasminogen activator inhibitor-1]) and *Il1b* (encoding IL1β). The latter set comprised *Tgfb1* (encoding TGFβ1), *Fn* (also known as *Fn1* [encoding fibronectin]), *Col4a3* (encoding type IV collagen alpha 3 chain), *Ctgf* (encoding connective tissue growth factor [CTGF]) and *Mmp2* (encoding matrix metalloproteinase 2). We found that expression levels of these genes in glomeruli and whole kidney were mildly elevated in WT STZ-ND compared with WT nSTZ-ND mice, in general (Fig. 2, ESM Table 3). Gene expression levels were further upregulated in WT STZ-HFD animals. Of note, differences between nSTZ-HFD and nSTZ-ND groups were

Fig. 1 Treatment of STZ diabetic mice with an HFD worsens renal injury in WT but not in *Tlr4* KO mice. (a, b) Addition of HFD to STZ mice causes similar degrees of deposition of lipid droplets staining positive with Oil Red O in WT (white bars) and KO mice (black bars) at 16 weeks of age. Magnification $\times 4$. Data are means \pm SEM. $n=5$. *** $p<0.001$. Time course of urinary albumin levels normalised with urinary creatinine levels in WT (c) and *Tlr4* KO mice (d). Circles, nSTZ-ND; triangles, nSTZ-HFD; squares, STZ-ND; diamonds, STZ-HFD. W, weeks after STZ injection. $n=6-10$. † $p<0.05$ vs WT STZ-ND, † $p<0.05$ vs WT STZ-HFD calculated by area under the curve. (e, f) Immunofluorescence analysis of glomerular podocin level. White bars, WT; black bars, KO; $n=4-6$. * $p<0.05$, ** $p<0.01$, *** $p<0.001$. † $p<0.05$ for similarly treated KO vs WT



negligible (Fig. 2). Histological analysis also showed that MAC-2-positive-macrophage infiltration into glomeruli (Fig. 3a) and renal interstitium (ESM Fig. 2) and glomerular mesangial expansion (Fig. 3b) in STZ-HFD mice were markedly more pronounced than in STZ-ND mice.

Screening of candidate genes involved in the pathogenesis of diabetic nephropathy To identify candidate molecules potentially involved in the pathophysiology of diabetic nephropathy, we analysed gene expression profiles of diabetic mouse glomeruli by microarray (ESM Table 4). We compared two types of diabetic nephropathy from STZ-induced and A-ZIP/F-1 lipotrophic diabetes mice. We selected commonly regulated genes to minimise interference from the renal toxicity of STZ, genetic background [22] and direct insulin or leptin target molecules [23]. The list of genes commonly upregulated in these two models included pro-

inflammatory and ECM-associated genes and also ones encoding TLRs (ESM Table 4). As pairs of cell surface receptors and their ligands provide attractive seeds for future therapeutic targets, we focused on TLR4, for which glomerular levels were elevated by 1.7-fold by STZ and 5.8-fold in A-ZIP/F-1 compared with each control by microarray. We further examined the expression of genes encoding molecules reported to be endogenous ligands for TLR4 [7], and identified *S100a8* (also known as *Mrp8*) and *S100a9* (also known as *Mrp14*) [24], for which glomerular gene expression was commonly upregulated in two models of diabetic nephropathy by microarray (ESM Table 4). Upregulation of *Tlr4* and *S100a8* gene expression in glomeruli of STZ and A-ZIP/F-1 mice was confirmed by quantitative RT-PCR (ESM Fig. 3a, b). Moreover, in STZ-HFD mice, expression of these genes was further potentiated compared with other groups such as STZ-ND and nSTZ-HFD, especially in

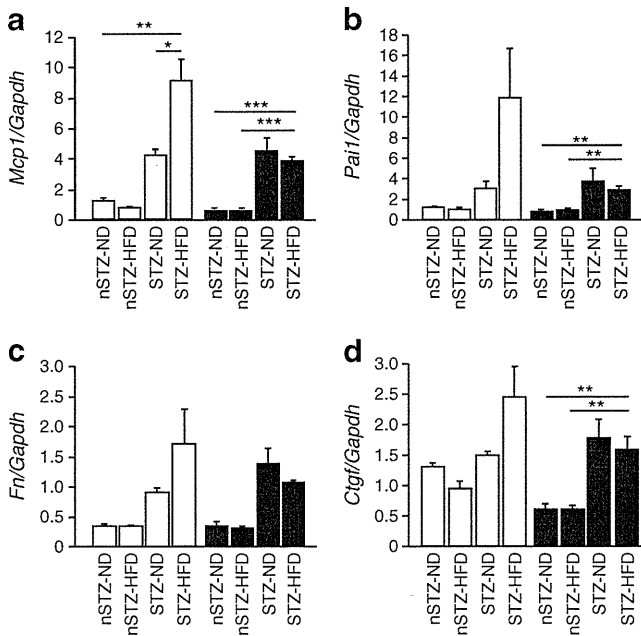


Fig. 2 Treatment with STZ and HFD synergistically upregulates inflammatory and ECM-associated gene expression in glomeruli of WT mice by real-time RT-PCR, but the effects of HFD are largely blunted in *Tlr4* KO mice: (a) *Mcp1*; (b) *Pai1*; (c) *Fn*; and (d) *Ctgf*. White bars, WT; black bars, KO. Data are means±SEM. *n*=4–11. **p*<0.05, ***p*<0.01, ****p*<0.001

glomeruli (Fig. 4a), but not in whole kidney (ESM Fig. 4). However, there was no significant increase in the expression of genes encoding other endogenous ligands for TLR4, such as *Hmgb1*, at the same time in both STZ and A-ZIP/F-1 mice compared with their respective controls, as assessed by

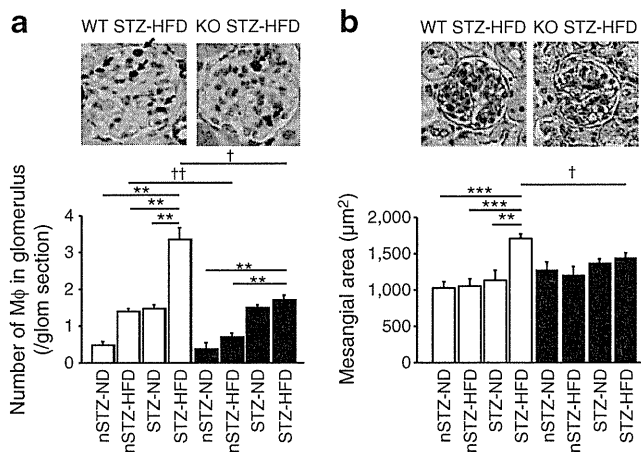


Fig. 3 Glomerular macrophage infiltration and mesangial matrix accumulation are markedly enhanced in WT mice co-treated with STZ and HFD, but not in *Tlr4* KO mice. **a** Macrophage (Mφ) number per glomerular (glom) section determined by MAC-2 immunostaining (arrows). Magnification ×40. Data are means±SEM. *n*=4–5. **b** Glomerular mesangial area determined by PAS staining (purple). Magnification ×20. *n*=4–6. White bars, WT; black bars, KO. ***p*<0.01, ****p*<0.001. †*p*<0.05, ††*p*<0.01 for similarly treated KO vs WT

microarray (ESM Table 4) or by quantitative RT-PCR (ESM Fig. 3c, d).

Production of S100A8 protein in diabetic kidney We performed immunohistochemical analyses of S100A8 protein in the kidneys both in STZ-HFD mice and human biopsy samples. In mice, abundance of S100A8 protein, in a punctate pattern, was observed predominantly in glomeruli of WT STZ-HFD mice, while S100A8 abundance was much lower in glomeruli of nSTZ-ND, nSTZ-HFD and STZ-ND groups (Fig. 4b, ESM Fig. 5). S100A8 protein was also detected in the interstitium of STZ-HFD mice but less abundantly than in the glomeruli. Double immunostaining revealed that 86% of S100A8 signals co-localised with macrophage marker MAC-2 in the glomeruli of STZ-HFD mice (Fig. 4c). In humans, S100A8 was abundantly detected in the glomeruli of patients with diabetic nephropathy, but not obviously in glomeruli of minor glomerular abnormality or minimal change nephrotic syndrome cases (Fig. 5).

Effects of *Tlr4* defect on STZ-HFD mice and on BMDMs To elucidate a functional role played by TLR4 in the progression of diabetic nephropathy accelerated by diet-induced hyperlipidaemia, we investigated the effects of STZ and HFD in *Tlr4* KO mice. In baseline nSTZ-ND conditions, KO mice showed significantly heavier body weights compared with WT mice, paralleled by mildly elevated plasma levels of glucose, insulin, triacylglycerol and total cholesterol in KO mice (Table 1). Plasma glucose levels in KO nSTZ-HFD mice were slightly lower compared with their WT counterparts. These findings are consistent with previous observations indicating that, compared with WT mice, *Tlr4* KO mice are prone to accumulation of fat but resistant to development of insulin resistance when challenged with an HFD [25, 26]. When STZ-HFD conditions were compared between KO and WT mice, the levels of plasma glucose and total cholesterol and renal lipid deposition were similar among the genotypes, and plasma triacylglycerol levels tended to be higher in KO than WT mice (Table 1, Fig. 1b). On the other hand, exacerbation of albuminuria and suppression of glomerular podocin protein production resulting from HFD treatment in WT STZ mice were all largely blunted in KO STZ animals (Fig. 1c–f). Additionally, infiltrated macrophage counts in glomeruli and renal interstitium and mesangial expansion were remarkably smaller in KO STZ-HFD mice than in WT STZ-HFD mice (Fig. 3, ESM Fig. 2). Furthermore, upregulation of pro-inflammatory (*Mcp1* and *Pai1*), pro-fibrotic (*Fn* and *Ctgf*), *S100a8* and *S100a9* gene expression and S100A8-positive cell counts caused by HFD treatment in glomeruli of WT STZ mice were almost completely abolished in KO STZ mice (Figs 2 and 4a, b, ESM Fig. 5). These findings indicate that, despite similar degrees of metabolic abnormalities caused

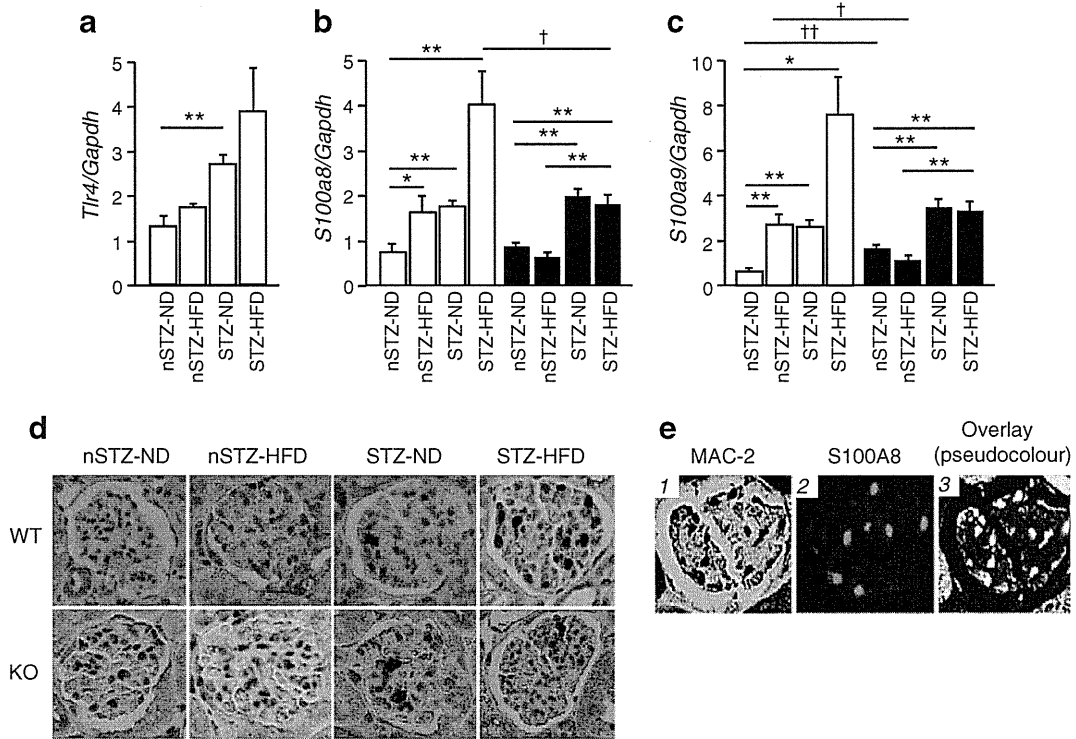


Fig. 4 Glomerular expression of *Tlr4*, *S100a8* and *S100a9* mRNA and S100A8 protein is markedly upregulated in WT STZ-HFD but not in *Tlr4* KO STZ-HFD mice, and S100A8 is predominantly produced by glomerular macrophages in WT STZ-HFD mice. **a–c** Gene expression of *Tlr4* (**a**), *S100a8* (**b**) and *S100a9* (**c**) in glomeruli, determined by real-time RT-PCR. White bars, WT; black bars, KO. Data are means±SEM. $n=4-11$. * $p<0.05$, ** $p<0.01$. † $p<0.05$, †† $p<0.01$ for similarly

treated KO vs WT. **d** Glomerular S100A8 protein (brown) examined by immunohistochemistry. Magnification×40. **e** Localisation of MAC-2 (brown in panel 1, pseudocoloured with green in panel 3, by immunohistochemistry), S100A8 (red in panels 2 and 3, by immunofluorescence) and their overlaps (yellow in panel 3) in glomeruli of WT STZ-HFD mice

by diabetes and hyperlipidaemia, *Tlr4* KO mice developed much less severe renal lesions compared with WT mice.

With regard to comparison between WT and *Tlr4* KO mice treated with STZ alone (STZ-ND mice), urinary albumin excretion (Fig. 1c, d), glomerular podocin production (Fig. 1e, f), glomerular gene expression of *Mcp1*, *Pai1*, *, *Ctgf*, *S100a8*, and *S100a9* (Figs 2 and 4a), and glomerular macrophage infiltration (Fig. 3a) were all similar among two genotypes, suggesting that *Tlr4* does not strongly participate in early and mild changes of diabetic nephropathy. Concerning HFD treatment alone (nSTZ-HFD mice), there were no significant differences in urinary albumin excretion and glomerular podocin production between WT and KO*

mice (Fig. 1c–f), while glomerular *S100a9* gene expression (Fig. 4a) and glomerular macrophage infiltration (Fig. 3a) were significantly attenuated in KO compared with WT mice, suggesting that treatment solely with HFD significantly activated circulating macrophages in WT mice but the TLR4-mediated signal in nSTZ-HFD mice was not sufficient to cause functional changes in the glomeruli.

To gain insights into how the combination of diabetes and hyperlipidaemia resulted in markedly enhanced migration of macrophages into glomeruli, we examined BMDMs. We focused attention on expression of a potent TLR4 ligand, S100A8 [24]. Treatment of WT macrophages with a fatty acid, palmitate, induced *S100a8* mRNA upregulation when the cells were cultured in high-glucose conditions, but upregulation was not observed under low-glucose conditions (Fig. 6a). Furthermore, induction of *S100a8* expression by palmitate in high-glucose-treated macrophages did not occur in cells from *Tlr4* KO animals (Fig. 6b). High-glucose treatment slightly increased *Tlr4* expression in WT macrophages (Fig. 6c).

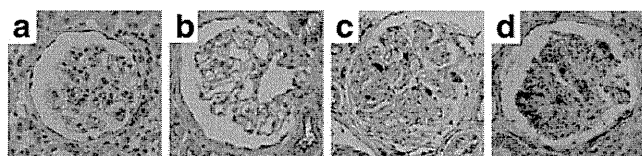


Fig. 5 S100A8 (brown) is observed in glomeruli of patients with diabetic nephropathy by immunohistochemistry: **(a)** minor glomerular abnormality; **(b)** minimal change nephrotic syndrome; and **(c)** and **(d)** severe cases of diabetic nephropathy

TLR4 signalling in the kidney of STZ-HFD model To examine the TLR4-downstream signalling cascade, we performed

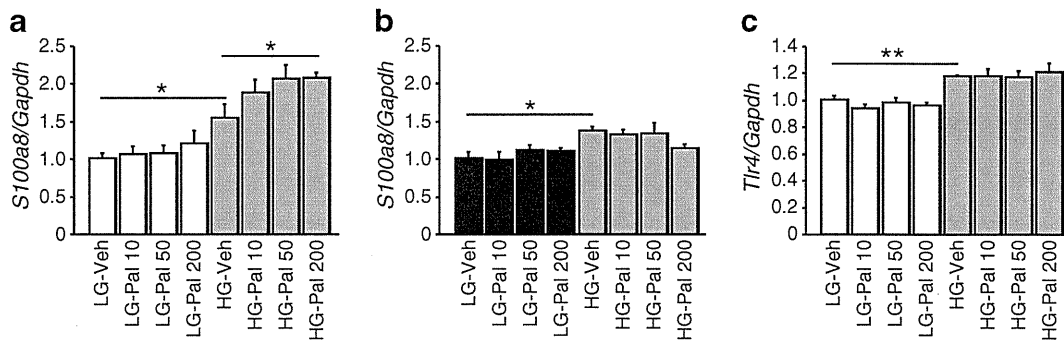


Fig. 6 *S100a8* expression in BMDMs is synergistically induced by high glucose and palmitate in a *Tlr4*-dependent manner. **a** *S100a8* mRNA expression by real-time RT-PCR in BMDMs from WT mice cultured under low-glucose (5.6 mmol/l, white bars) or high-glucose (25 mmol/l, grey bars) conditions and effects of palmitate (10–200 μ mol/l). Data are means \pm SEM. $n=6$. **b** *S100a8* mRNA expression

in BMDMs from *Tlr4* KO mice cultured under low-glucose (black bars) or high-glucose (grey bars) conditions and the effects of palmitate. $n=6$. **c** *Tlr4* mRNA expression in WT BMDMs. $n=6$. * $p < 0.05$, ** $p < 0.01$. LG, low glucose; HG, high glucose; pal, palmitate; Veh, vehicle

western blot analyses of key adaptor proteins and transcription factors which have been reportedly classified into myeloid differentiation primary response gene (88) (MYD88)-dependent, TIR-domain-containing adapter-inducing interferon- β (TRIF)-dependent or common pathways (Fig. 7a) [7], using whole kidney lysate. Treatment of WT STZ mice with HFD was associated with increased phosphorylation of inhibitor of κ B (IKB) and c-Jun N-terminal kinase (JNK) in a common pathway, and with increased phosphorylation of interferon regulatory factor 3 (IRF3) in a TRIF-dependent pathway, but not with increased protein production of TNF receptor-associated factor 6 (TRAF6) nor increased phosphorylation of interleukin-1-receptor-associated kinase (IRAK) in the MYD88-dependent pathway (Fig. 7b–e). PCR array analysis, which allows simultaneous evaluation of relevant genes involved in the signalling cascades of TLR1–TLR9, confirmed that in WT STZ-HFD kidneys, TRIF-dependent pathway-inducible genes (*Cxcl10*, *Ifnb1* [encoding interferon β 1] and *Cd80*) and common pathway-inducible genes (*Mcp1*) were highly upregulated, but genes involved in the MYD88-dependent pathway (*Cd14*, *Ly96* [encoding myeloid differentiation protein-2 {MD-2}], and *Traf6*) were not changed compared with WT STZ-ND kidneys (ESM Table 5). Furthermore, disruption of the *Tlr4* gene markedly blocked the activation of the putative TLR4 downstream signalling cascade in STZ-HFD mice (Fig. 7b–e, ESM Table 5).

Discussion

In the present study, we have revealed that treatment of WT mice with STZ combined with HFD synergistically aggravated renal lesions, indicated by enhancement of albuminuria, macrophage infiltration, mesangial expansion and pro-inflammatory/ECM-associated gene induction in glomeruli. These changes were accompanied with upregulation of a

TLR4 ligand, S100A8, and activation of putative TRIF-dependent pathway downstream of TLR4. In *Tlr4* KO mice, the addition of HFD to STZ had almost no effect on kidney damage, suggesting that TLR4 plays an important role in the exacerbation of diabetic nephropathy by hyperlipidaemia.

Of note, treatment with STZ alone caused similar and mild renal changes in WT and KO mice, suggesting that the TLR4 signal may not significantly participate in the onset of diabetic nephropathy at 8 weeks after STZ injection [13]. However, WT mice fed with HFD (nSTZ-HFD) exhibited significantly higher levels of *S100a9* gene expression and more macrophage infiltration in glomeruli compared with KO mice, but these effects were not reflected in differences in other renal lesion variables, suggesting that macrophage activation in nSTZ-HFD mice may require longer observation periods than were used in this study in order to be functionally relevant.

Here, to study the effects of an HFD on diabetes, we used a lean model of type 1 diabetes to avoid introducing complexity through alterations in insulin resistance and fat accumulation with the HFD or by *Tlr4* gene disruption in the type 2 diabetes model [19, 20]. The HFD-induced and hypertriacylglycerolaemia-associated renal injury observed in this study may have been caused through activation of TLR4 by NEFA [25, 26], oxidised LDL [27], or triacylglycerol-rich lipoproteins [6]. Previous studies have proposed that, by direct lipotoxicity on tubular epithelial cells, diet-induced obesity alone is sufficient to cause inflammatory and fibrotic changes in the whole kidney preparations through gene expression of *Cd36* or *sterol regulatory element-binding protein-1c* (*Srebp1c*) [28–30]. In the present study, however, treatment of WT mice solely with HFD resulted in very mild renal lesions, probably because we used a diet with a lower fat content and studied the mice for a shorter period of time compared with earlier reports [28–30]. Furthermore, HFD increased glomerular *Cd36* mRNA expression but STZ-induced

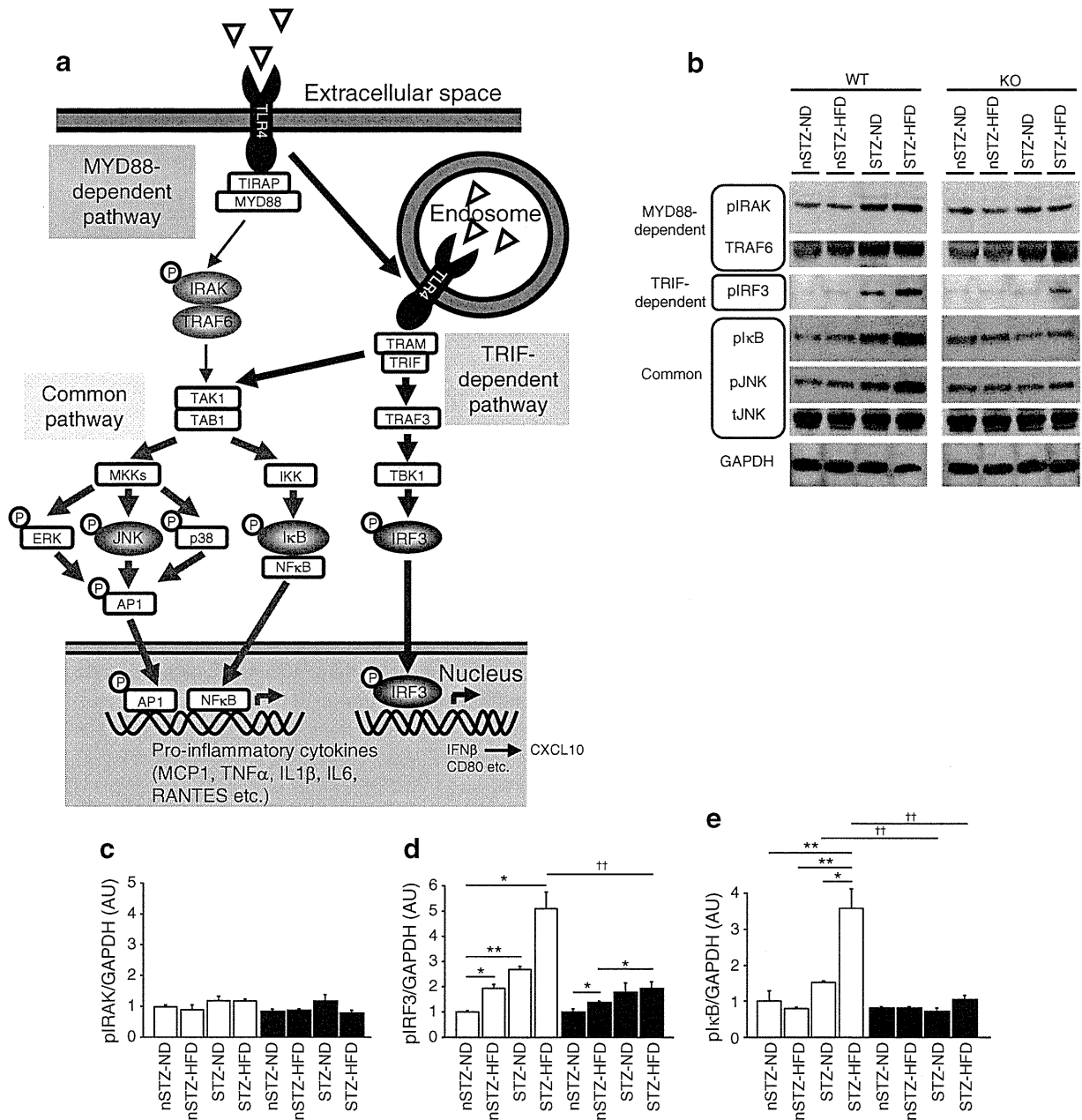


Fig. 7 Exacerbation of STZ-induced diabetic nephropathy by HFD is associated with increased phosphorylation of proteins involved in TRIF-dependent and common pathways of the TLR4 signalling cascade in WT kidney but not in *Tlr4* KO kidney. **a** Schema describing the known TLR4 signalling cascade. The common pathway can be activated both through MYD88-dependent and TRIF-dependent pathways. Key molecules analysed in (b) are highlighted as elliptical objects. **b–e** Western blot analyses of TLR4 signalling and quantitative evaluation. White bars, WT; black bars, KO. Data are means±SEM. $n=4$. * $p<0.05$, ** $p<0.01$. †† $p<0.01$ for similarly treated KO vs WT. AP1, jun proto-oncogene; AU, arbitrary units; CXCL10, chemokine (C-X-C motif) ligand 10; ERK, mitogen-

activated protein kinase 1; (p)IKB, (phosphorylated) inhibitor of κB ; IKK, inhibitor of kappa light polypeptide gene enhancer in B cells, kinase; (p)IRAK, (phosphorylated) interleukin-1 receptor-associated kinase 1; pIRF3, phosphorylated IRF3; (p)(t)JNK, (phosphorylated)/(total) JNK; MKKs, mitogen-activated protein kinase kinases; p38, mitogen-activated protein kinase 14; RANTES, chemokine (C-C motif) ligand 5; TAB1, TGFβ-activated kinase 1/MAP3K7 binding protein 1; TAK1, nuclear receptor subfamily 2, group C, member 2; TBK1, TANK-binding kinase 1; TIRAP, Toll-interleukin 1 receptor domain containing adaptor protein; TRAF3, TNF receptor-associated factor 3; TRAM, translocation associated membrane protein 1

diabetes reduced it, and glomerular *Srebplc* expression was decreased both by HFD and STZ (ESM Fig. 6), indicating that HFD-induced exacerbation of diabetic nephropathy cannot be explained by upregulation of CD36 or SREBP1C.

S100A8 forms a heterodimer with S100A9, and the complex is one of the most powerful endogenous ligands for TLR4, which is essential for full activation of macrophages and other leucocytes, by a positive feedback loop, during

endotoxin-induced shock and vascular and autoimmune disorders [24, 31, 32]. TLR4 signalling also plays an important role in the development of various kidney diseases, yet the role of TLR4 in diabetic glomerulopathy or hyperlipidaemia-induced kidney damage remains to be elucidated [8–13]. Recently, Burkhardt et al and Bouma et al reported that serum S100A8/A9 complex concentrations were elevated in patients with diabetes [33, 34]. In our study, S100A8 protein was abundant in the glomeruli of mice given STZ and HFD and also in glomeruli of patients with diabetic nephropathy, and was mainly produced by macrophages. Furthermore, we found that high glucose and NEFA treatments, when combined, markedly upregulated *S100a8* expression in WT macrophages, but not in *Tlr4* KO macrophages. These findings suggest that production of S100A8 is not just an indicator of systemic inflammation but may play a pathogenic role in the deterioration of diabetic nephropathy. Functional analysis of S100A8 protein production in diabetic mice is currently under way in our laboratory. Candidate *Tlr4*-expressing cells in the diabetic kidney include macrophages, podocytes and mesangial and tubular epithelial cells [8, 9]. So far, we have been unable to obtain reliable findings by immunohistochemistry using commercially available antibodies for TLR4, and we are now trying other methods. Of note, upregulation of *S100a8* gene expression by HFD in STZ mice was also observed in the liver and aorta, suggesting that the effects of these treatments are not specifically targeted to the kidney but are systemic (ESM Fig. 6). HMGB1 is one of endogenous ligands of TLR4 [9], and AGE-specific receptor (AGER or RAGE) is one of the S100A8 receptors so far identified [35]. Although mRNA expression of these molecules in glomeruli was not upregulated in diabetic mice in this study (ESM Fig. 3, ESM Table 4), we cannot exclude the possibility that they are involved in hyperlipidaemia-induced renal injury.

The macrophage has been presumed to be a critical mediator of diabetic nephropathy [36–38], and blockade of the MCP-1/CC chemokine receptor 2 system in diabetic mice leads to reduced albuminuria, mesangial expansion and macrophage infiltration [39–42]. Secretory factors from macrophages may cause histological and functional changes in glomeruli. For example, TGF β 1 (TGFB1) and MCP1, induced in surrounding cells by or secreted directly from activated macrophages, have been shown to upregulate CTGF production [43] and increase albumin permeability in cultured podocytes [44–46]; we have recently reported that overproduction of CTGF specifically in podocytes is sufficient to worsen diabetic nephropathy [19].

Downstream signalling of TLR4 has been divided into MYD88-dependent and TRIF-dependent pathways, leading to early- and late-phase nuclear factor of κ light polypeptide gene enhancer in B cells 1 (NF κ B) activation, respectively [7]. In addition, endocytosed TLR4 activates the TRIF-dependent pathway [47]. It is interesting to determine

whether pathologically accumulated lipids in endosomes of macrophages can cause chronic inflammation via the TRIF-dependent pathway in the kidneys of STZ-HFD mice. Here, in STZ-HFD kidneys, we observed an increase in IRF3 protein phosphorylation and *Cxcl10*, *Ifnb1* and *Cd80* mRNA expression, reported to be in the TRIF-dependent pathway, but experiments blocking TRIF activity are required to demonstrate the TRIF dependency of the process.

In conclusion, we have elucidated a novel mechanism of hyperlipidaemia-induced renal damage in diabetic conditions in a TLR4-dependent manner that appears to involve the activation of a S100A8/TLR4 signalling pathway in glomeruli. Further investigation is required to see whether this signalling cascade is relevant in the progression of nephropathy in diabetic patients.

Acknowledgements We acknowledge S. Akira (WPI Immunology Frontier Research Center, Osaka University, Suita, Japan) for kindly providing us with *Tlr4* KO mice. We gratefully acknowledge Y. Ogawa and A. Yamamoto and other laboratory members for their assistance.

Funding This work was supported in part by Grant-in-Aid for Diabetic Nephropathy Research (K. Mori), research grants from the Japanese Ministry of Education, Culture, Sports, Science and Technology (T. Kuwabara, K. Mori and M. Mukoyama) and from the Smoking Research Foundation (M. Mukoyama).

Duality of interest The authors declare that there is no duality of interest associated with this manuscript.

Contribution statement All authors contributed to the conception and design, or analysis and interpretation of data, and drafting the article or revising it critically for important intellectual content, and have given final approval of the version to be published.

References

1. Maisonneuve P, Agodoa L, Gellert R et al (2000) Distribution of primary renal diseases leading to end-stage renal failure in the United States, Europe, and Australia/New Zealand: results from an international comparative study. *Am J Kidney Dis* 35:157–165
2. Decleves AE, Sharma K (2010) New pharmacological treatments for improving renal outcomes in diabetes. *Nat Rev Nephrol* 6:371–380
3. El-Atat FA, Stas SN, McFarlane SI, Sowers JR (2004) The relationship between hyperinsulinemia, hypertension and progressive renal disease. *J Am Soc Nephrol* 15:2816–2827
4. Perkins BA, Ficociello LH, Silva KH, Finkelstein DM, Warram JH, Krolewski AS (2003) Regression of microalbuminuria in type 1 diabetes. *N Engl J Med* 348:2285–2293
5. Ravid M, Brosh D, Ravid-Safran D, Levy Z, Rachmani R (1998) Main risk factors for nephropathy in type 2 diabetes mellitus are plasma cholesterol levels, mean blood pressure, and hyperglycemia. *Arch Intern Med* 158:998–1004
6. Rutledge JC, Ng KF, Aung HH, Wilson DW (2010) Role of triglyceride-rich lipoproteins in diabetic nephropathy. *Nat Rev Nephrol* 6:361–370

7. Akira S, Takeda K (2004) Toll-like receptor signalling. *Nat Rev Immunol* 4:499–511
8. Brown HJ, Lock HR, Wolfs TG, Buurman WA, Sacks SH, Robson MG (2007) Toll-like receptor 4 ligation on intrinsic renal cells contributes to the induction of antibody-mediated glomerulonephritis via CXCL1 and CXCL2. *J Am Soc Nephrol* 18:1732–1739
9. Wu H, Chen G, Wyburn KR et al (2007) TLR4 activation mediates kidney ischemia/reperfusion injury. *J Clin Invest* 117:2847–2859
10. Zhang B, Ramesh G, Uematsu S, Akira S, Reeves WB (2008) TLR4 signaling mediates inflammation and tissue injury in nephrotoxicity. *J Am Soc Nephrol* 19:923–932
11. Liu B, Yang Y, Dai J et al (2006) TLR4 up-regulation at protein or gene level is pathogenic for lupus-like autoimmune disease. *J Immunol* 177:6880–6888
12. Kruger B, Krick S, Dhillon N et al (2009) Donor Toll-like receptor 4 contributes to ischemia and reperfusion injury following human kidney transplantation. *Proc Natl Acad Sci USA* 106:3390–3395
13. Lin M, Yiu WH, Wu HJ et al (2012) Toll-like receptor 4 promotes tubular inflammation in diabetic nephropathy. *J Am Soc Nephrol* 23:86–102
14. Hoshino K, Takeuchi O, Kawai T et al (1999) Cutting edge: Toll-like receptor 4 (TLR4)-deficient mice are hyporesponsive to lipopolysaccharide: evidence for TLR4 as the Lps gene product. *J Immunol* 162:3749–3752
15. Kuwabara T, Mori K, Mukoyama M et al (2009) Urinary neutrophil gelatinase-associated lipocalin levels reflect damage to glomeruli, proximal tubules, and distal nephrons. *Kidney Int* 75:285–294
16. Kusakabe T, Tanioka H, Ebihara K et al (2009) Beneficial effects of leptin on glycaemic and lipid control in a mouse model of type 2 diabetes with increased adiposity induced by streptozotocin and a high-fat diet. *Diabetologia* 52:675–683
17. Jung K, Wesslau C, Priem F, Schreiber G, Zubek A (1987) Specific creatinine determination in laboratory animals using the new enzymatic test kit "Creatinine-PAP". *J Clin Chem Clin Biochem* 25:357–361
18. Suganami T, Mukoyama M, Sugawara A et al (2001) Overexpression of brain natriuretic peptide in mice ameliorates immune-mediated renal injury. *J Am Soc Nephrol* 12:2652–2663
19. Yokoi H, Mukoyama M, Mori K et al (2008) Overexpression of connective tissue growth factor in podocytes worsens diabetic nephropathy in mice. *Kidney Int* 73:446–455
20. Suganami T, Mukoyama M, Mori K (2005) Prevention and reversal of renal injury by leptin in a new mouse model of diabetic nephropathy. *FASEB J* 19:127–129
21. Suganami T, Yuan X, Shimoda Y et al (2009) Activating transcription factor 3 constitutes a negative feedback mechanism that attenuates saturated Fatty acid/toll-like receptor 4 signaling and macrophage activation in obese adipose tissue. *Circ Res* 105:25–32
22. Qi Z, Fujita H, Jin J et al (2005) Characterization of susceptibility of inbred mouse strains to diabetic nephropathy. *Diabetes* 54:2628–2637
23. Vaisse C, Halaas JL, Horvath CM, Damell JE Jr, Stoffel M, Friedman JM (1996) Leptin activation of Stat3 in the hypothalamus of wild-type and ob/ob mice but not db/db mice. *Nat Genet* 14:95–97
24. Vogl T, Tenbrock K, Ludwig S et al (2007) Mrp8 and Mrp14 are endogenous activators of Toll-like receptor 4, promoting lethal, endotoxin-induced shock. *Nat Med* 13:1042–1049
25. Suganami T, Mieda T, Itoh M, Shimoda Y, Kamei Y, Ogawa Y (2007) Attenuation of obesity-induced adipose tissue inflammation in C3H/HeJ mice carrying a Toll-like receptor 4 mutation. *Biochem Biophys Res Commun* 354:45–49
26. Shi H, Kokoeva MV, Inouye K, Zmamiel I, Yin H, Flier JS (2006) TLR4 links innate immunity and fatty acid-induced insulin resistance. *J Clin Invest* 116:3015–3025
27. Xu XH, Shah PK, Faure E et al (2001) Toll-like receptor-4 is expressed by macrophages in murine and human lipid-rich atherosclerotic plaques and upregulated by oxidized LDL. *Circulation* 104:3103–3108
28. Kume S, Uzu T, Araki S et al (2007) Role of altered renal lipid metabolism in the development of renal injury induced by a high-fat diet. *J Am Soc Nephrol* 18:2715–2723
29. Okamura DM, Pennathur S, Pasichnyk K et al (2009) CD36 regulates oxidative stress and inflammation in hypercholesterolemic CKD. *J Am Soc Nephrol* 20:495–505
30. Jiang T, Wang Z, Proctor G et al (2005) Diet-induced obesity in C57BL/6J mice causes increased renal lipid accumulation and glomerulosclerosis via a sterol regulatory element-binding protein-1c-dependent pathway. *J Biol Chem* 280:32317–32325
31. Croce K, Gao H, Wang Y et al (2009) Myeloid-related protein-8/14 is critical for the biological response to vascular injury. *Circulation* 120:427–436
32. Loser K, Vogl T, Voskort M et al (2010) The Toll-like receptor 4 ligands Mrp8 and Mrp14 are crucial in the development of autoreactive CD8+ T cells. *Nat Med* 16:713–717
33. Burkhardt K, Schwarz S, Pan C et al (2009) Myeloid-related protein 8/14 complex describes microcirculatory alterations in patients with type 2 diabetes and nephropathy. *Cardiovasc Diabetol* 8:10
34. Bouma G, Lam-Tse WK, Wierenga-Wolf AF, Drexhage HA, Versnel MA (2004) Increased serum levels of MRP-8/14 in type 1 diabetes induce an increased expression of CD11b and an enhanced adhesion of circulating monocytes to fibronectin. *Diabetes* 53:1979–1986
35. Yamamoto Y, Kato I, Doi T et al (2001) Development and prevention of advanced diabetic nephropathy in RAGE-overexpressing mice. *J Clin Invest* 108:261–268
36. Furuta T, Saito T, Ootaka T et al (1993) The role of macrophages in diabetic glomerulosclerosis. *Am J Kidney Dis* 21:480–485
37. Sassy-Prigent C, Heudes D, Mandet C et al (2000) Early glomerular macrophage recruitment in streptozotocin-induced diabetic rats. *Diabetes* 49:466–475
38. Usui HK, Shikata K, Sasaki M et al (2007) Macrophage scavenger receptor-a-deficient mice are resistant against diabetic nephropathy through amelioration of microinflammation. *Diabetes* 56:363–372
39. Chow FY, Nikolic-Paterson DJ, Ozols E, Atkins RC, Rollin BJ, Tesch GH (2006) Monocyte chemoattractant protein-1 promotes the development of diabetic renal injury in streptozotocin-treated mice. *Kidney Int* 69:73–80
40. Chow FY, Nikolic-Paterson DJ, Ma FY, Ozols E, Rollins BJ, Tesch GH (2007) Monocyte chemoattractant protein-1-induced tissue inflammation is critical for the development of renal injury but not type 2 diabetes in obese db/db mice. *Diabetologia* 50:471–480
41. Kanamori H, Matsubara T, Mima A et al (2007) Inhibition of MCP-1/CCR2 pathway ameliorates the development of diabetic nephropathy. *Biochem Biophys Res Commun* 360:772–777
42. Sayyed SG, Ryu M, Kulkarni OP et al (2011) An orally active chemokine receptor CCR2 antagonist prevents glomerulosclerosis and renal failure in type 2 diabetes. *Kidney Int* 80:68–78
43. Yokoi H, Mukoyama M, Sugawara A et al (2002) Role of connective tissue growth factor in fibronectin expression and tubulointerstitial fibrosis. *Am J Physiol Renal Physiol* 282:F933–942
44. Takano Y, Yamauchi K, Hayakawa K et al (2007) Transcriptional suppression of nephrin in podocytes by macrophages: roles of inflammatory cytokines and involvement of the PI3K/Akt pathway. *FEBS Lett* 581:421–426
45. Lee EY, Chung CH, Khoury CC et al (2009) The monocyte chemoattractant protein-1/CCR2 loop, inducible by TGF-beta, increases podocyte motility and albumin permeability. *Am J Physiol Renal Physiol* 297:F85–94
46. Kwok C, Shannon MB, Miner JH, Shaw A (2006) Pathogenesis of nonimmune glomerulopathies. *Annu Rev Pathol* 1:349–374
47. Kagan JC, Su T, Hornig T, Chow A, Akira S, Medzhitov R (2008) TRAM couples endocytosis of Toll-like receptor 4 to the induction of interferon-beta. *Nat Immunol* 9:361–368

Intracerebroventricular Administration of C-Type Natriuretic Peptide Suppresses Food Intake via Activation of the Melanocortin System in Mice

Nobuko Yamada-Goto,¹ Goro Katsuura,¹ Ken Ebihara,¹ Megumi Inuzuka,¹ Yukari Ochi,¹ Yui Yamashita,¹ Toru Kusakabe,¹ Akihiro Yasoda,¹ Noriko Satoh-Asahara,² Hiroyuki Ariyasu,¹ Kiminori Hosoda,¹ and Kazuwa Nakao¹

C-type natriuretic peptide (CNP) and its receptor are abundantly distributed in the brain, especially in the arcuate nucleus (ARC) of the hypothalamus associated with regulating energy homeostasis. To elucidate the possible involvement of CNP in energy regulation, we examined the effects of intracerebroventricular administration of CNP on food intake in mice. The intracerebroventricular administration of CNP-22 and CNP-53 significantly suppressed food intake on 4-h refeeding after 48-h fasting. Next, intracerebroventricular administration of CNP-22 and CNP-53 significantly decreased nocturnal food intake. The increment of food intake induced by neuropeptide Y and ghrelin was markedly suppressed by intracerebroventricular administration of CNP-22 and CNP-53. When SHU9119, an antagonist for melanocortin-3 and melanocortin-4 receptors, was coadministered with CNP-53, the suppressive effect of CNP-53 on refeeding after 48-h fasting was significantly attenuated by SHU9119. Immunohistochemical analysis revealed that intracerebroventricular administration of CNP-53 markedly increased the number of c-Fos-positive cells in the ARC, paraventricular nucleus, dorsomedial hypothalamus, ventromedial hypothalamic nucleus, and lateral hypothalamus. In particular, c-Fos-positive cells in the ARC after intracerebroventricular administration of CNP-53 were coexpressed with α -melanocyte-stimulating hormone immunoreactivity. These results indicated that intracerebroventricular administration of CNP induces an anorexigenic action, in part, via activation of the melanocortin system. *Diabetes* 62:1500–1504, 2013

C-type natriuretic peptide (CNP) is a member of the natriuretic peptide family and has been demonstrated to be abundantly present in the brain, interestingly in discrete hypothalamic areas, such as the arcuate nucleus (ARC) of the hypothalamus, that play pivotal roles in energy regulation (1–3). Two predominant molecular forms of CNP in the porcine brain were reported to be a 22-residue peptide (CNP-22) and its N-terminally elongated 53-residue peptide (CNP-53) (1). Moreover, natriuretic peptide receptor-B (NPR-B), a CNP receptor, is also widely distributed in the brain and is reported to be abundantly expressed in the ARC of the

hypothalamus (4,5). These findings indicate the possibility that the brain CNP/NPR-B system may regulate energy homeostasis.

In the current study, we examined the effects of intracerebroventricular administration of CNP on food intake induced by refeeding after fasting and by orexigenic peptides, such as neuropeptide Y (NPY) and ghrelin. Also, we examined the involvement of the melanocortin system in the CNP actions.

RESEARCH DESIGN AND METHODS

Animals and diets. Male C57BL/6J mice (6 weeks old) obtained from Japan SLC (Shizuoka, Japan) were housed in plastic cages in a room kept at a room temperature of $23 \pm 1^\circ\text{C}$ and a 12:12-h light–dark cycle (lights turned on at 9:00 A.M.). The mice had ad libitum access to water and food (CE-2; CLEA Japan, Tokyo, Japan). All experiments were performed at 10 weeks of age in accordance with the guidelines established by the Institutional Animal Investigation Committee at Kyoto University and the United States National Institutes of Health Guide for the Care and Use of Laboratory Animals. Every effort was made to optimize comfort and to minimize the use of animals.

Peptides. CNP-22, CNP-53, ghrelin, and NPY were purchased from Peptide Institute (Osaka, Japan). SHU9119 was purchased from Bachem AG (Bubendorf, Switzerland).

Intracerebroventricular injection. Intracerebroventricular injection was performed according to our previous report (6).

Measurement of food intake

Fasting-refeeding. Mice were fasted for 48 h and then refed for 4 h. Water was available ad libitum during the experiments. The intracerebroventricular or intraperitoneal administration of CNP-22 or CNP-53 was performed just before refeeding. Food intake was measured for 4 h of refeeding. At the end of experiments, the hypothalamus was collected for examination of the expressions of mRNA for neuropeptides (7).

Nocturnal food intake. To assess the effect of intracerebroventricular administration of CNP-22 or CNP-53 on nocturnal food intake, peptides were injected intracerebroventricularly 1 h before the beginning of the dark phase. Food intake was measured for 15 h after intracerebroventricular injection. Water was available ad libitum during the experiments.

Food intake induced by NPY and ghrelin. The experiments were performed from 11:00 A.M. to 3:00 P.M. CNP-22 or CNP-53 was intracerebroventricularly administered just before intracerebroventricular injection of NPY (5 nmol/mouse) or intraperitoneal injection of ghrelin (100 nmol/kg). Food intake was measured for 4 h after peptide injection. In these experiments, food and water were available ad libitum.

PCR. The extraction of mRNA and quantitative real-time RT-PCR were performed according to our previous report (8). Primers for prepro-melanocortin, cocaine and amphetamine-related peptide, NPY, agouti gene-related peptide (*AgRP*) and glyceraldehyde 3-phosphate dehydrogenase are shown in Supplementary Table 1.

Immunohistochemistry for c-Fos and α -MSH in the hypothalamus. The immunohistochemical methods and the stereotaxic coordinates for the hypothalamic nuclei were based on our previous report (6). Briefly, mice were anesthetized with pentobarbital at 1 h after intracerebroventricular injection of CNP-53 (1.5 nmol/mouse) and perfused with 50 mL 0.1 mol/L PBS, followed by 50 mL ice-cold 4% paraformaldehyde in 0.1 mol/L PBS. Sections of 30- μm thickness were cut with a cryostat. According to the mouse brain atlas (9), cross-sections were selected in correspondence to -1.70 mm [ARC, lateral hypothalamus (LH), dorsomedial hypothalamus (DMH), ventromedial hypothalamic

From the ¹Department of Medicine and Clinical Science, Kyoto University Graduate School of Medicine, Kyoto, Japan; and the ²Clinical Research Institute, National Hospital Organization, Kyoto Medical Center, Kyoto, Japan. Corresponding author: Nobuko Yamada-Goto, nobukito@kuhp.kyoto-u.ac.jp. Received 31 May 2012 and accepted 7 November 2012. DOI: 10.2337/db12-0718

This article contains Supplementary Data online at <http://diabetes.diabetesjournals.org/lookup/suppl/doi:10.2337/db12-0718/-/DC1>.

© 2013 by the American Diabetes Association. Readers may use this article as long as the work is properly cited, the use is educational and not for profit, and the work is not altered. See <http://creativecommons.org/licenses/by-nc-nd/3.0/> for details.

See accompanying commentary, p. 1379.

nucleus (VMH) and to -0.82 mm [paraventricular nucleus (PVN)], relative to bregma. For c-Fos and α -melanocyte-stimulating hormone (α -MSH) protein staining, the sections were incubated with anti-c-Fos rabbit antibody (Ab-5; 1:5,000; Oncogene Science, Cambridge, MA) and anti- α -MSH sheep antibody (AB5087; 1:10,000; EMD Millipore, Billerica, MA), respectively. The antibody was detected using the Vectastain ABC Elite kit (PK-6101; Vector Laboratories, Burlingame, CA) and a diaminobenzidine substrate kit (SK-4100; Vector Laboratories) was used for visualization. The second antibodies for fluorescence visualization used were goat anti-rabbit488 (A11008; 1:200; Life Technologies, Carlsbad, CA) for anti-c-Fos rabbit antibody and goat anti-sheep546 (A21098; 1:200; Life Technologies) for anti- α -MSH sheep antibody.

Data analysis. All values are given as the mean \pm SEM. Statistical analysis of the data were performed by ANOVA, followed by the Tukey-Kramer test. Statistical significance was defined as $P < 0.05$.

RESULTS

Effects of intracerebroventricular administration of CNP-22 and CNP-53 on food intake at refeeding after fasting. The intracerebroventricular administration of CNP-22 (1.5 and 4.5 nmol/mouse) and CNP-53 (1.5 nmol/mouse) significantly suppressed food intake during 4-h refeeding after 48-h fasting in comparison with data from saline-treated mice (Fig. 1A). In this experiment, CNP-53 (1.5 nmol), but not other treatments, induced significant reduction of body weight compared with saline treatment (Supplementary Table 2). The mRNA expressions of pre- α -melanocortin and cocaine and amphetamine-related peptide significantly decreased, and the mRNA expressions of *NPY* and *AgRP* significantly increased after refeeding compared with control animals (Supplementary Fig. 1). The intracerebroventricular administration of CNP-53 did not influence the mRNA expressions of these neuropeptides in the hypothalamus (Supplementary Fig. 1). Next, the peripheral action of CNP on food intake was examined when a 10-fold greater dose than intracerebroventricular injection of each CNP was intraperitoneally administered. The intraperitoneal administrations of CNP-22 (1.5 μ mol/kg) and CNP-53 (0.5 μ mol/kg) did not change the food intake during 4-h refeeding after 48-h fasting (Fig. 1B), nor were there changes in body weight (Supplementary Table 3).

The intracerebroventricular administrations of CNP-22 (4.5 nmol/mouse) and CNP-53 (1.5 nmol/mouse) at 1 h before the start of the dark phase significantly suppressed nocturnal food intake compared with saline treatment (Fig. 1C).

Effect of intracerebroventricular administration of CNP-22 and CNP-53 on NPY-induced and ghrelin-induced food intake. When CNP-22 (4.5 nmol/mouse) and CNP-53 (1.5 nmol/mouse) were concomitantly administered intracerebroventricularly with NPY, they significantly suppressed the food intake induced by NPY compared with that of saline treatment (Fig. 2A). When CNP-22 (4.5 nmol/mouse) and CNP-53 (1.5 nmol/mouse) were administered intracerebroventricularly with ghrelin, they significantly suppressed the food intake induced by ghrelin compared with that of saline treatment (Fig. 2B). **Effect of melanocortin receptor antagonist, SHU9119, on the anorectic effect of CNP.** To examine its involvement in the anorectic effect of CNP, SHU9119 was administered intracerebroventricularly together with CNP-53 (1.5 nmol/mouse). SHU9119 (1 nmol/mouse) significantly attenuated the suppressive action of CNP-53 on the food intake during 4-h refeeding after 48-h fasting, whereas SHU9119 itself significantly enhanced the increase of food intake in comparison with mice administered saline treatment (Fig. 3).

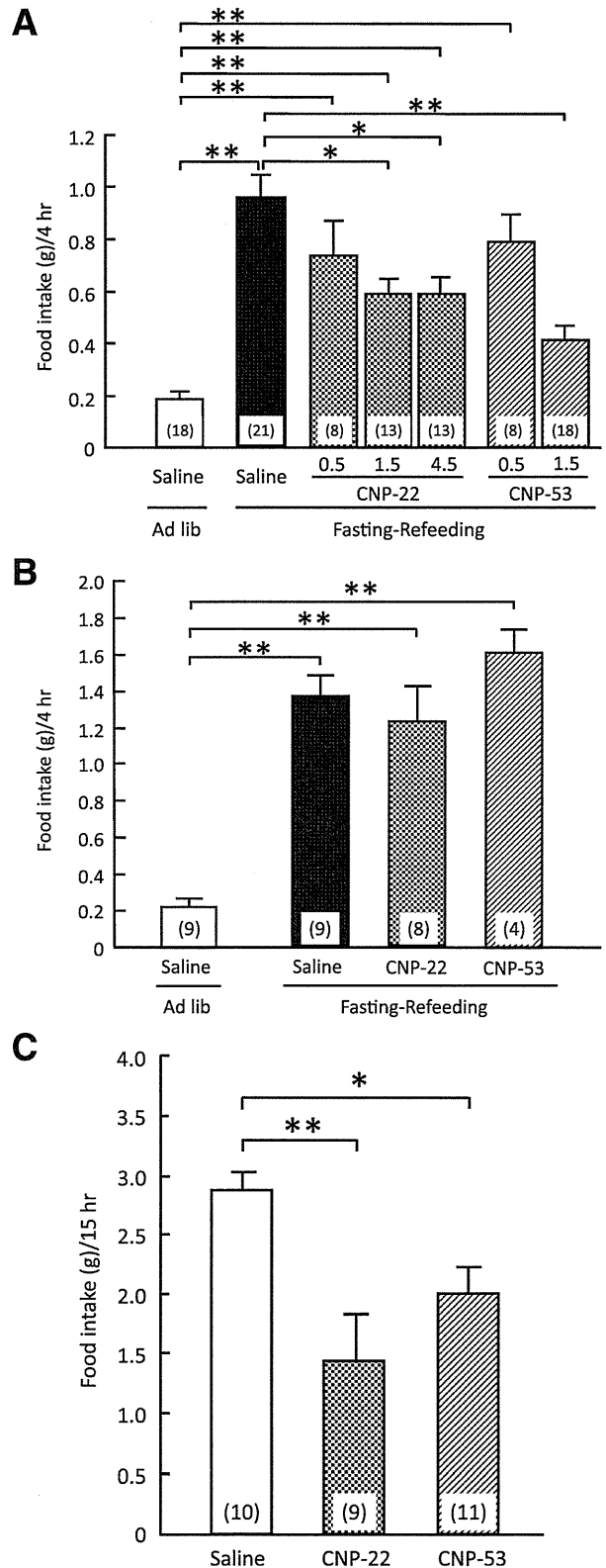


FIG. 1. Effects of CNP on refeeding after fasting. **A:** Effects of intracerebroventricular administration of CNP-22 (0.5, 1.5, and 4.5 nmol/mouse) and CNP-53 (0.5 and 1.5 nmol/mouse) on 4-h refeeding after 48-h fasting in mice. Food intake was observed for 4 h after refeeding. **B:** Effects of intraperitoneal administration of CNP-22 (1.5 μ mol/kg) and CNP-53 (0.5 μ mol/kg) on 4-h refeeding after 48-h fasting in mice. Food intake was observed for 4 h after refeeding. **C:** Effects of intracerebroventricular administration of CNP-22 (4.5 nmol/mouse) and CNP-53 (1.5 nmol/mouse) on nocturnal food intake in mice. Food intake was observed for 15 h after intracerebroventricular injection. Data represent mean \pm SEM. The number of mice is given in parentheses. Significant differences: * $P < 0.05$, ** $P < 0.01$.

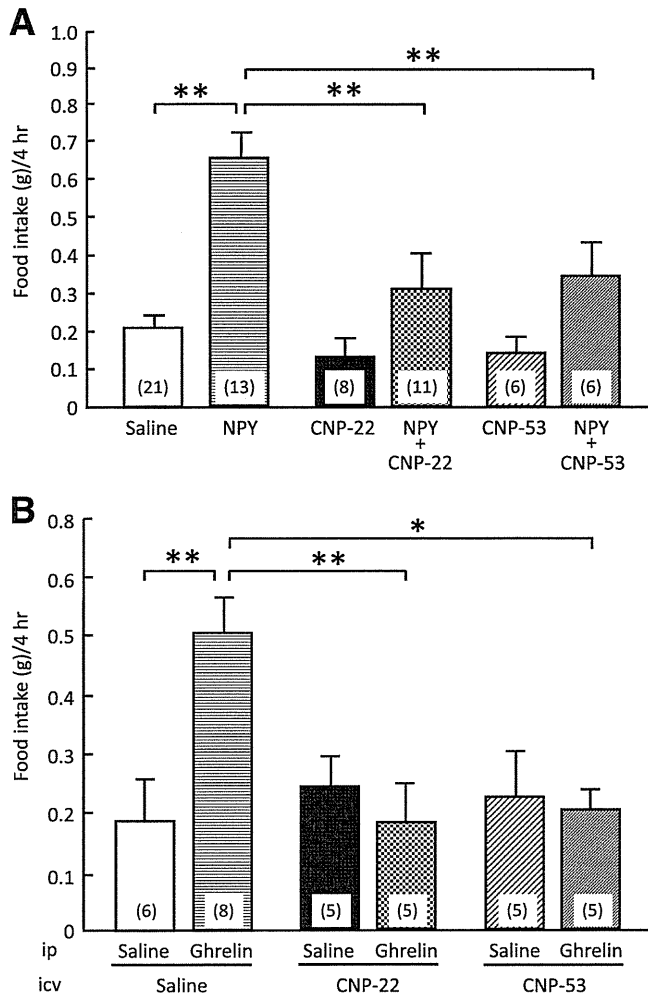


FIG. 2. Effects of CNP-22 and CNP-53 on food intake induced by NPY and ghrelin. **A:** Effects of intracerebroventricular administration of CNP-22 (4.5 nmol/mouse) and CNP-53 (1.5 nmol/mouse) on NPY-induced (5 nmol/mouse, intracerebroventricular) food intake in mice. Food intake was observed for 4 h after coadministration of NPY and CNP. **B:** Effects of intracerebroventricular administration of CNP-22 (4.5 nmol/mouse) and CNP-53 (1.5 nmol/mouse) on ghrelin-induced (100 nmol/kg, intraperitoneal) food intake in mice. Food intake was observed for 4 h after coadministration of ghrelin and CNP. Data represent mean \pm SEM. The number of mice is given in parentheses. Significant differences: * $P < 0.05$, ** $P < 0.01$.

c-Fos-immunoreactive cells in the hypothalamus after intracerebroventricular administration of CNP.

To understand the neuronal pathway involved in the anorectic actions of CNP, the expression of c-Fos, one of the markers of neuronal activation, was monitored by immunohistochemical examination at 1 h after intracerebroventricular injection of CNP-53 (1.5 nmol/mouse). The numbers of c-Fos-immunoreactive cells in the ARC, PVN, and DMH were predominantly increased after intracerebroventricular injection of CNP-53 in comparison with saline treatment (Fig. 4A). The c-Fos-positive cells were also moderately increased in the VMH and LH (Fig. 4A). Next, we examined whether c-Fos immunoreactivity coexisted with α -MSH-containing cells. In the ARC of saline-treated mice, only a few α -MSH-immunoreactive cells showed weak c-Fos immunoreactivity (Fig. 4B). However, c-Fos-immunoreactive cells that increased with intracerebroventricular administration of CNP-53 in the ARC expressed a large amount of α -MSH immunoreactivity (Fig. 4B).

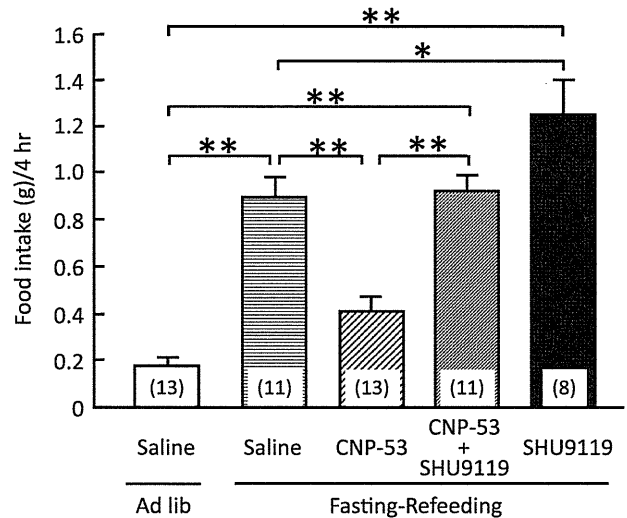


FIG. 3. Effects of intracerebroventricular administration of CNP-53 (1.5 nmol/mouse) and SHU9119 (1 nmol/mouse) on refeeding after 48-h fasting in mice. Food intake was observed for 4 h after refeeding. Data represent mean \pm SEM. The number of mice is given in parentheses. Significant differences: * $P < 0.05$, ** $P < 0.01$.

DISCUSSION

The current study demonstrated that intracerebroventricular administration of CNP-22 and CNP-53, but not intraperitoneal injection, led to significant reduction of food intake induced by fasting–refeeding. This reduction was inhibited by the melanocortin-3 receptor (MC3R)/melanocortin-4 receptor (MC4R) antagonist SHU9119. In addition, CNP significantly suppressed nocturnal food intake and orexigenic actions induced by NPY and ghrelin. The immunohistochemical study revealed that intracerebroventricular administration of CNP-53 increased the number of c-Fos-expressing cells containing α -MSH in the hypothalamus. These findings indicated that the intracerebroventricular administration of CNP exhibits anorexic actions partially via activation of the melanocortin system, although the doses of CNP used in the current study could be pharmacological doses.

The hypothalamus is considered to be an important region in regulating energy homeostasis. In particular, the ARC in the hypothalamus contains both an orexigenic peptide, NPY, and an anorexic peptide, α -MSH, and is postulated to be involved in the first-order regulation of food intake. Synthetic MC3R/MC4R agonists, melanotan II, and [Nle⁴-D-Phe⁷]- α -MSH completely blocked food deprivation-induced increase in food intake as well as the food intake stimulated by intracerebroventricular administration of NPY (10,11). Regarding the reciprocal interactions of α -MSH and NPY, melanocortin neurons in the ARC project to the PVN (12). In the current study, intracerebroventricular administration of CNP significantly suppressed food intake after fasting, which was antagonized by SHU9119. Our results also showed that CNP suppressed NPY-induced food intake. Taken together, these findings indicate that CNP exhibits anorexic actions via activation of MC3R/MC4R downstream signaling. However, mRNA expressions of prepro-melanocortin, cocaine and amphetamine-related peptide, NPY, and *AgRP* in the hypothalamus after the intracerebroventricular injection of CNP-53 in fasting–refeeding experiment did not change compared with those after saline. The reason for this

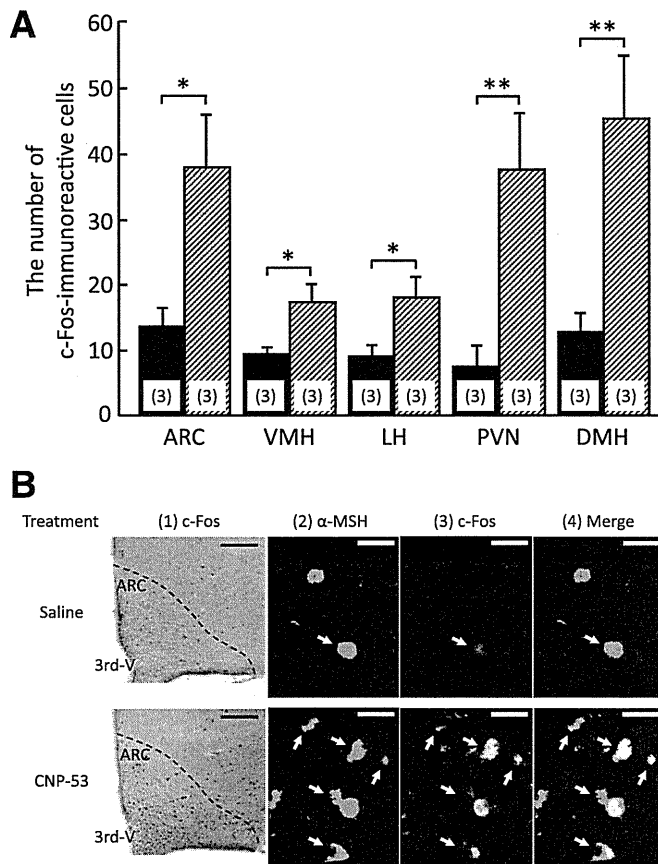


FIG. 4. The c-Fos-immunoreactive cells in the hypothalamus after intracerebroventricular administration of CNP-53 (1.5 nmol/mouse). **A:** Number of c-Fos-immunoreactive cells after saline and CNP-53 treatments. Data represent mean \pm SEM. The number of mice is given in parentheses. Significant differences: * $P < 0.05$, ** $P < 0.01$. **B:** c-Fos-immunoreactive cells induced by intracerebroventricular administration of saline and CNP-53 (1). 3rd-V, the third ventricular. Scale bars, 100 μ m. Coexistence of α -MSH (red) and c-Fos (green) immunoreactivity in the ARC (2–4) after saline (upper) and CNP-53 (1.5 nmol/mouse; lower) treatments. White arrows indicate cells expressing both α -MSH and c-Fos immunoreactivity. 3rd-V, the third ventricular. Scale bars, 20 μ m.

discrepancy may lie in the experimental condition, time course, and regional specificity. To clarify this discrepancy, further examinations will be required.

This study demonstrated that the intracerebroventricular administration of CNP significantly suppressed the nocturnal food intake. Robust feeding during the nocturnal phase of the daily light–dark cycle was demonstrated to be attributed to the upregulation of NPY and its receptors (13). These findings indicate that CNP may decrease food intake in the nocturnal phase via suppression of NPY action.

In the current study, CNP significantly suppressed the increase in food intake induced by ghrelin, an orexigenic hormone secreted by the stomach (14). NPR-B, a CNP receptor, has been identified in appetite-regulating regions, such as the ARC, VMH, PVN, DMH, and LH (15). The systemic administration of ghrelin significantly increased NPY and AgRP expression in the ARC of the hypothalamus in fed and fasted rats (15), resulting in hyperphagia. The intracerebroventricular injection of melanotan II caused a significant decrease in ghrelin-induced food intake (16). These findings suggest that the actions of ghrelin are modulated by α -MSH and NPY systems. Furthermore, plasma ghrelin and hypothalamic ghrelin receptor mRNA

expression are reported to be increased after fasting (17,18). These findings suggest the possibility that intracerebroventricular administration of CNP activates the melanocortin system, which subsequently inhibits the action of NPY, resulting in a reduced increase of food intake induced by ghrelin.

To assess which hypothalamic nucleus is involved in the anorexigenic action of CNP, a marker for neuronal activity, c-Fos expression in the hypothalamus was examined after intracerebroventricular administration of CNP-53. The intracerebroventricular administration of CNP-53 significantly increased the number of c-Fos-expressing cells in several hypothalamic nuclei, such as ARC, PVN, DMH, VMH, and LH, indicating that CNP-53 directly or indirectly stimulates neurons in these hypothalamic nuclei. Especially in the ARC, the result was an increased number of c-Fos-immunoreactive cells containing α -MSH immunoreactivity, indicating that CNP stimulates α -MSH-containing neurons. This possibility is supported by the finding that the suppressive action of CNP-53 on food intake was blocked by concomitant administration of SHU9119, an MC3R/MC4R antagonist.

The current study has demonstrated the anorexigenic action of intracerebroventricular administration of CNP via activation of the melanocortin system. To define the precise effect of CNP in the brain on food intake, further investigation using mice with inducible brain-specific deletion of CNP or NPR-B/NPR-C will be required.

From the present findings, we postulate the possible mechanism for anorexigenic action of exogenous CNP to be as follows: CNP directly or indirectly acts on α -MSH-containing neurons and subsequently stimulates α -MSH release, resulting in suppression of food intake induced by NPY and ghrelin. This possible mechanism may apply to the suppressive effects of CNP on food intake after fasting and in the nocturnal phase. Further work is needed to define the pathophysiological significance of brain CNP in regulation of food intake.

ACKNOWLEDGMENTS

This work was supported in part by research grants from the Ministry of Education, Culture, Sports, Science, and Technology of Japan, and the Ministry of Health, Labour, and Welfare of Japan.

No potential conflicts of interest relevant to this article were reported.

N.Y.-G. and G.K. performed experiments, contributed to discussion, and wrote the manuscript. K.E., M.I., Y.O., Y.Y., T.K., A.Y., N.S.-A., H.A., and K.H. contributed to discussion. K.N. contributed to discussion, and reviewed and edited the manuscript. K.N. is the guarantor of this work and, as such, had full access to all the data in the study and takes responsibility for the integrity of the data and the accuracy of the data analysis.

REFERENCES

1. Minamino N, Makino Y, Tateyama H, Kangawa K, Matsuo H. Characterization of immunoreactive human C-type natriuretic peptide in brain and heart. *Biochem Biophys Res Commun* 1991;179:535–542
2. Herman JP, Langub MC Jr, Watson RE Jr. Localization of C-type natriuretic peptide mRNA in rat hypothalamus. *Endocrinology* 1993;133:1903–1906
3. Langub MC Jr, Watson RE Jr, Herman JP. Distribution of natriuretic peptide precursor mRNAs in the rat brain. *J Comp Neurol* 1995;356:183–199
4. Langub MC Jr, Dolgas CM, Watson RE Jr, Herman JP. The C-type natriuretic peptide receptor is the predominant natriuretic peptide receptor mRNA expressed in rat hypothalamus. *J Neuroendocrinol* 1995;7:305–309

5. Herman JP, Dolgas CM, Rucker D, Langub MC Jr. Localization of natriuretic peptide-activated guanylate cyclase mRNAs in the rat brain. *J Comp Neurol* 1996;369:165-187
6. Yamada N, Katsuura G, Ochi Y, Ebihara K, Kusakabe T, Hosoda K, Nakao K. Impaired CNS leptin action is implicated in depression associated with obesity. *Endocrinology* 2011;152:2634-2643
7. Nakao K, Katsuura G, Morii N, Itoh H, Shiono S, Yamada T, Sugawara A, Sakamoto M, Saito Y, Eigyo M, Matsushita A, Imura H. Inhibitory effect of centrally administered atrial natriuretic polypeptide on the brain dopaminergic system in rats. *Eur J Pharmacol* 1986;131:171-177
8. Yamada N, Katsuura G, Tatsuno I, et al. Orexin decreases mRNA expressions of NMDA and AMPA receptor subunits in rat primary neuron cultures. *Peptides* 2008;29:1582-1587
9. Paxinos G, Franklin KBJ. *The mouse brain in stereotaxic coordinates*. New York, Academic Press, 2004
10. Brown KS, Gentry RM, Rowland NE. Central injection in rats of alpha-melanocyte-stimulating hormone analog: effects on food intake and brain Fos. *Regul Pept* 1998;78:89-94
11. Murphy B, Nunes CN, Ronan JJ, et al. Melanocortin mediated inhibition of feeding behavior in rats. *Neuropeptides* 1998;32:491-497
12. Sánchez E, Singru PS, Acharya R, et al. Differential effects of refeeding on melanocortin-responsive neurons in the hypothalamic paraventricular nucleus. *Endocrinology* 2008;149:4329-4335
13. Kalra PS, Dube MG, Xu B, Farmerie WG, Kalra SP. Evidence that dark-phase hyperphagia induced by neurotoxin 6-hydroxydopamine may be due to decreased leptin and increased neuropeptide Y signaling. *Physiol Behav* 1998;63:829-835
14. Kojima M, Hosoda H, Date Y, Nakazato M, Matsuo H, Kangawa K. Ghrelin is a growth-hormone-releasing acylated peptide from stomach. *Nature* 1999;402:656-660
15. Harrold JA, Dovey T, Cai XJ, Halford JC, Pinkney J. Autoradiographic analysis of ghrelin receptors in the rat hypothalamus. *Brain Res* 2008;1196:59-64
16. Shrestha YB, Wickwire K, Giraudo SQ. Action of MT-II on ghrelin-induced feeding in the paraventricular nucleus of the hypothalamus. *Neuroreport* 2004;15:1365-1367
17. Keen-Rhinehart E, Bartness TJ. NPY Y1 receptor is involved in ghrelin- and fasting-induced increases in foraging, food hoarding, and food intake. *Am J Physiol Regul Integr Comp Physiol* 2007;292:R1728-R1737
18. Kim MS, Yoon CY, Park KH, et al. Changes in ghrelin and ghrelin receptor expression according to feeding status. *Neuroreport* 2003;14:1317-1320